IMMUNOLOGY

Single-cell transcriptomics identifies multiple pathways underlying antitumor function of TCR- and CD8αβ-engineered human CD4$^+$ T cells

Jan A. Rath[1]*, Gagan Bajwa[2]*, Benoit Carreres[1], Elisabeth Hoyer[2], Isabelle Gruber[1], Melisa A. Martínez-Paniagua[3], Yi-Ru Yu[1], Nazila Nouraee[2], Fatemeh Sadeghi[3], Mengfen Wu[4], Tao Wang[4], Michael Hebeisen[1], Nathalie Rufer[1], Navin Varadarajan[3], Ping-Chih Ho[1], Malcolm K. Brenner[2,5,6,7], David Gfeller[1], Caroline Arber[1,2,5†]

Transgenic coexpression of a class I–restricted tumor antigen–specific T cell receptor (TCR) and CD8αβ (TCR8) redirects antigen specificity of CD4$^+$ T cells. Reinforcement of biophysical properties and early TCR signaling explain how redirected CD4$^+$ T cells recognize target cells, but the transcriptional basis for their acquired antitumor function remains elusive. We, therefore, interrogated redirected human CD4$^+$ and CD8$^+$ T cells by single-cell RNA sequencing and characterized them experimentally in bulk and single-cell assays and a mouse xenograft model. TCR8 expression enhanced CD8$^+$ T cell function and preserved less differentiated CD4$^+$ and CD8$^+$ T cells after tumor challenge. TCR8$^+$CD4$^+$ T cells were most potent by activating multiple transcriptional programs associated with enhanced antitumor function. We found sustained activation of cytotoxicity, costimulation, oxidative phosphorylation– and proliferation-related genes, and simultaneously reduced differentiation and exhaustion. Our study identifies molecular features of TCR8 expression that can guide the development of enhanced immunotherapies.

INTRODUCTION

Naturally occurring major histocompatibility complex (MHC) class I–restricted T cell receptors (TCRs) targeting tumor-associated antigens (TAAs) often depend on the presence of the CD8αβ coreceptor to stabilize their limited functional avidity. To enable the recruitment of beneficial CD4$^+$ T cells with class I TCR–based adoptive T cell therapies, transgenic coexpression of CD8αβ and TCR (TCR8) has been evaluated as a strategy to redirect CD4$^+$ T cells to the tumor (*1*–*6*). Although reinforcement of biophysical properties during TCR-MHC (peptide-MHC) recognition and early TCR signaling were suggested as potential mechanisms for enhanced functionality, it is unknown whether forced TCR8 expression induces more fundamental transcriptional consequences in CD4$^+$ or CD8$^+$ T cells.

CD8αβ coreceptor function has been extensively studied over the past decades. It exerts multiple crucial roles during the TCR-pMHC recognition and T cell activation processes (*7*, *8*) that include stabilization of the TCR-pMHC complex by binding to MHC class I molecules (*9*–*11*), delivery of key signaling components to the cytoplasmic side of the TCR/CD3 complex (*12*, *13*), and partitioning the TCR in the optimal membrane compartment for signal transduction (*13*–*15*). TCR dependency on the CD8αβ coreceptor correlates with TCR affinity, and thus, CD8αβ has the capacity to modulate the antigen sensitivity of low-affinity TCR T cells over several log fold (*16*–*18*). All these functions have the potential to substantially affect the outcome of adoptive T cell therapy with TCR-engineered T cells (*1*–*6*). In addition, the presence of functional CD4$^+$ T cells is indispensable for the orchestration of an effective immune response as they make multifaceted contributions to antigen-specific immunity to viral infections and are prerequisite for the initiation and maintenance of long-term tumor control (*19*). For example, antigen-specific CD4$^+$ T cells are required for long-term benefit in patients receiving virus-specific T cells, tumor-infiltrating lymphocytes, or chimeric antigen receptor (CAR) T cells (*20*–*22*).

In this study, we aimed to deeply interrogate the functional and transcriptional effects of forced transgenic CD8αβ expression together with a previously identified CD8-dependent TCR that targets survivin (TCR8) in CD4$^+$ and CD8$^+$ T cells (*23*). We hypothesized that (i) TCR8-redirected CD4$^+$ and CD8$^+$ T cells are functionally and transcriptionally distinct even though both are cytotoxic against the targeted class I epitope, (ii) single-cell transcriptomics will identify differential pathway usage and T cell differentiation status, and (iii) combining transgenic expression of CD8αβ with TCR modifies the function and transcriptome of transgenic CD8$^+$ T cells, not only CD4$^+$ T cells. For this purpose, we investigated single T cell transcriptomics of engineered CD4$^+$ and CD8$^+$ T cells and corroborated our findings with functional assays in vitro and in vivo.

We found that redirected CD4$^+$ T cells killed relevant target cells when transduced with TCR8 but not TCR alone, and their cytotoxicity, cytokine production, and biophysical properties were comparable to TCR$^+$CD8$^+$ or TCR8$^+$CD8$^+$ T cells. Single-cell RNA sequencing (scRNAseq) analysis identified transcriptional effects related to T cell lineage (CD4$^+$ or CD8$^+$), cell state (fresh, expanded, or cocultured), or transgene type (TCR or TCR8). Lineage- and cell state–related effects were most pronounced. Cocultured TCR8$^+$CD4$^+$ T cells were characterized by sustained up-regulation of multiple transcriptional

[1]Department of Oncology UNIL-CHUV, Lausanne University Hospital, Ludwig Institute for Cancer Research, University of Lausanne, Lausanne, Switzerland. [2]Center for Cell and Gene Therapy, Baylor College of Medicine, Houston Methodist Hospital and Texas Children's Hospital, Houston, TX, USA. [3]Department of Chemical and Biomolecular Engineering, University of Houston, TX, USA. [4]Biostatistics Shared Resource, Dan L. Duncan Comprehensive Cancer Center, Baylor College of Medicine, Houston, TX, USA. [5]Department of Medicine, Baylor College of Medicine, Houston, TX, USA. [6]Department of Pediatrics, Baylor College of Medicine, Houston, TX, USA. [7]Department of Molecular and Human Genetics, Baylor College of Medicine, Houston, TX, USA.
*These authors contributed equally to this work and are co-first authors.
†Corresponding author. Email: caroline.arber@unil.ch

programs that have previously been associated with sustained antitumor responses of engineered T cells, such as antigen-dependent cytotoxicity and replication without terminal differentiation and exhaustion of T cells, costimulation, and metabolic fitness. In vivo in the leukemia mouse xenograft model, TCR8$^+$ transgenic T cells achieved better leukemia control than TCR$^+$ transgenic T cells (both CD4$^+$ and CD8$^+$), and TCR8$^+$CD4$^+$ T cells outperformed TCR8$^+$CD8$^+$ T cells.

RESULTS

Transgenic expression of TAA-specific class I–restricted TCR8 confers class I–directed antitumor function to CD4$^+$ T cells

Most TCRs targeting overexpressed tumor-associated self-antigens are characterized by CD8 coreceptor dependence, including our HLA-A*02:01–restricted survivin-specific TCR (*23*). To therapeutically exploit CD4$^+$ T cell functions in TCR$^+$ adoptive T cell therapy, we coexpressed the survivin-TCR (*23*) and CD8αβ chains in a polycistronic vector (TCR8) (Fig. 1A). We obtained high transduction efficiencies and cell surface expression of the relevant transgenes with both the TCR and TCR8 vectors (fig. S1, A to D). TCR$^+$CD4$^+$ T cells only minimally bound to the epitope-specific dextramer, but TCR8$^+$CD4$^+$ T cells showed comparable dextramer mean fluorescence intensities (MFIs) as TCR$^+$CD8$^+$ or TCR8$^+$CD8$^+$ T cells (fig. S1D). To measure the effect of transgenic CD8αβ on stabilization of the TCR in CD4$^+$ T cells, we performed TCR-pMHC dissociation measurements by NTAmer technology and fluorescence-activated cell sorting (FACS) (*24*, *25*). K_{off} rates in CD8$^+$ T cells were similar whether they were transduced with TCR or TCR8 (Fig. 1, B and C). In CD4$^+$ T cells, however, NTAmer binding was only detected when cells were transduced with TCR8, but not with TCR alone. The monomeric dissociation rates in TCR8$^+$CD4$^+$ T cells were equivalent to the kinetics measured in TCR$^+$CD8$^+$ or TCR8$^+$CD8$^+$ T cells (Fig. 1, B and C). Next, we analyzed LCK-Y394 phosphorylation upon stimulation of T cells with BV173 leukemia as a readout for early TCR signaling events. We found that activating pLCK-Y394 levels were significantly increased in TCR8$^+$CD8$^+$ T cells as well as TCR8$^+$CD4$^+$ T cells when compared with TCR$^+$CD8$^+$ or TCR$^+$CD4$^+$ T cells, respectively (Fig. 1, D and E). A trend toward increased pLCK levels in TCR8$^+$CD4$^+$ compared with TCR8$^+$CD8$^+$ T cells was also observed, but it was not statistically significant (Fig. 1E) This epitope-specific redirection conferred antigen sensitivity to CD4$^+$ T cells that was comparable to TCR$^+$CD8$^+$ or TCR8$^+$CD8$^+$ T cells [interferon-γ (IFN-γ) enzyme-linked immunospot (ELISpot); Fig. 1F]. In cocultures of T cells with survivin$^+$HLA-A*02:01$^+$ BV173 leukemia cells, we confirmed that TCR$^+$CD8$^+$ and TCR8$^+$CD8$^+$ T cells readily killed their targets. In contrast, CD4$^+$ T cells only killed when transduced with TCR8, but not with TCR alone. Killing by TCR8$^+$CD4$^+$ T cells was equivalent to TCR$^+$CD8$^+$ or TCR8$^+$CD8$^+$ T cells (TCR8$^+$CD4$^+$ versus TCR$^+$CD4$^+$, $P = 0.0004$; TCR8$^+$CD4$^+$ versus TCR$^+$CD8$^+$ or TCR8$^+$CD8$^+$, P = NS) (Fig. 1G). This cytotoxicity was HLA class I restricted, as redirected T cells only killed wild-type (WT) but not B2M-KO BV173 cells (Fig. 1H) that are surface HLA-A*02:01 negative. Thus, CD4$^+$ T cells were efficiently redirected to survivin by transgenic expression of TCR8, and these redirected TCR8$^+$CD4$^+$ T cells recapitulated functional features of TCR$^+$CD8$^+$ or TCR8$^+$CD8$^+$ T cells such as cytotoxicity or cytokine production.

Single-cell transcriptomics identifies distinct T cell subpopulations

Because the CD8αβ coreceptor modulates TCR activation, we investigated the transcriptional consequences of TCR8 in CD4$^+$ and CD8$^+$ T cells upon leukemia challenge (coculture) and explored the population heterogeneity in an unbiased approach. We performed scRNAseq on sorted human CD4$^+$ and CD8$^+$ T cells that were (i) freshly isolated, frozen, and thawed ("fresh," F); (ii) activated, transduced, selected, and expanded ("expanded," E); or (iii) expanded, cocultured, and cytotoxic to BV173 leukemia cells ("cocultured," C) (Fig. 2A).

t-Distributed scholastic neighbor embedding (t-SNE) analysis of the 25,474 single cells retained for analysis (table S1) partitioned cells into separate clusters broadly recapitulating the different cell types (CD4$^+$ or CD8$^+$ lineage) or cell states (fresh, expanded, or cocultured), although some additional substructures were visible (Fig. 2B). We observed extensive spatial overlap of expanded populations (green shading in Fig. 2B) within each lineage (e.g., TCR$^+$CD8$^+$ with TCR8$^+$CD8$^+$ T cells), suggesting little transcriptional impact of the inserted transgene during expansion. However, major transgene-dependent differences emerged upon coculture, leading to the clear separation of TCR$^+$CD8$^+$ from TCR8$^+$CD8$^+$ and TCR8$^+$CD4$^+$ T cells. To explore the cellular heterogeneity within each sample, we used k-nearest neighbor clustering and identified a total of 19 subpopulations (Fig. 2C and fig. S2) with distinct sets of differentially expressed (DE) genes (fig. S3).

To further investigate the transcriptional heterogeneity of cocultured T cells, we analyzed the top 20 DE genes of each cluster and revealed distinct transcriptional specificities (Fig. 2D and fig. S4). For instance, various cytotoxic genes differentially dominated CD4$^+$ and CD8$^+$ T cell clusters [e.g., *GZMB* in CD4$^+$ T cells (cluster 4) and *GNLY*, *CST7*, *NKG7*, and *GZMK* in CD8$^+$ T cells (clusters 9 and 12)]. *BHLHE40*, a key T helper cell 1 (T_H1)–associated transcription factor that controls cytokine production in activated CD4$^+$ T cells (*26*, *27*), was highly up-regulated in cocultured TCR8$^+$CD4$^+$ T cells (fig. S5A, left). A similar pattern was observed for the long noncoding RNA *MIR4435-2HG* that is important for cell cycle progression (fig. S5A, middle) (*28*). *RUNX3*, a crucial transcription factor for cytotoxic CD8$^+$ T cells and required for the acquisition of a cytotoxic phenotype in human virus–specific CD4$^+$ T cells (*29*), was stably expressed in TCR8$^+$CD4$^+$ and highly up-regulated in cocultured TCR8$^+$CD8$^+$ T cells (fig. S5A, right). Replicative populations of CD4$^+$ (cluster 14) and CD8$^+$ (cluster 18a and 18b) could be identified through the high expression of cell cycle genes (e.g., *CKS1b* and *CKS2*). TCR$^+$CD8$^+$ cells (clusters 6 and 12) were characterized by high levels of type I IFN–associated genes (e.g., *IFI6*) and chemokines (e.g., *XCL1*), indicating a strong effector cell differentiation. Naïve (T_N)– and central memory (T_{CM})–associated genes were enriched in cluster 4 (e.g., *MAL* and *CXCR4*) and cluster 7 (e.g., *TCF7* and *IL7R*) in a TCR8 transgene–dependent manner (Fig. 2D).

Next, we determined which genes were up-regulated from the expanded to cocultured states and summarized common or exclusive genes in a Venn diagram (Fig. 2E). We observed CD4$^+$ or CD8$^+$ T cell lineage–related as well as TCR8 transgene–related transcriptional changes that point toward potential mechanisms that underlie enhanced function of TCR8$^+$CD4$^+$ or TCR8$^+$CD8$^+$ T cells. The Venn analysis indicated that cocultured TCR8$^+$CD4$^+$ T cells had overall more up-regulated genes ($n = 212$) with a broader diversity compared with TCR$^+$CD8$^+$ ($n = 42$) or TCR8$^+$CD8$^+$ ($n = 41$) T cells. Among these up-regulated pathways were cytotoxicity, costimulation, oxidative phosphorylation (OXPHOS), nuclear factor κB (NF-κB) regulation, cell growth, and a variety of transcription factors. More

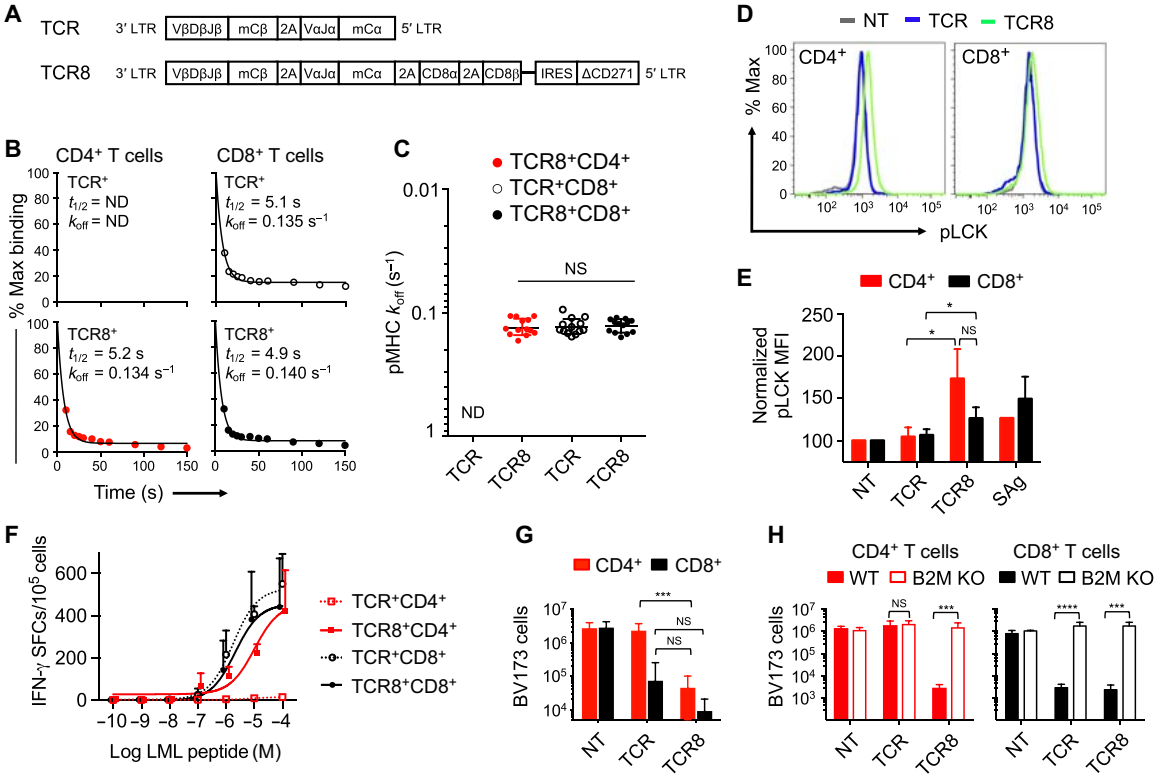

Fig. 1. Coexpression of CD8αβ with TCR redirects CD4$^+$ T cells to the targeted class I epitope. (**A**) Scheme of retroviral vectors containing the survivin-specific TCR (top, TCR) or the combination of TCR and CD8αβ and the selectable marker gene ΔCD271 (bottom, TCR8). (**B** and **C**) Determination of monomeric dissociation kinetics with survivin-specific reversible NTAmers. (**B**) Representative analysis of temperature-controlled (4°C) pMHC-TCR or pMHC-TCR8 monomeric dissociation rates. No NTAmer staining in TCR$^+$CD4$^+$ T cells; ND, not detected. (**C**) Summary of monomeric dissociation constants [k_{off} (s^{-1})], $n = 3$ donors, three independent experiments with technical replicates. Mean ± SD, P = NS, one-way analysis of variance (ANOVA) test. (**D** and **E**) Analysis of early TCR signaling events. (**D**) Representative FACS histograms of pLCK-Y394 phosphorylation NT (gray), TCR$^+$ (blue), and TCR8$^+$ (green) CD4$^+$ or CD8$^+$ T cells. (**E**) Summary of pLCK MFI normalized to MFI in NT control cells. $n = 4$ donors, mean ± SD, CD4: TCR$^+$ versus TCR8$^+$: 104 ± 11% versus 173 ± 35%, CD8: TCR$^+$ versus TCR8$^+$: 106 ± 7% versus 126 ± 13%, TCR8$^+$ CD8 versus CD4: 126 ± 13% versus 173 ± 35%. NS, not significant, *$P < 0.05$. (**F**) Antigen sensitivity measured by IFN-γ ELISpot against peptide-pulsed T2 cells. SFC, spot-forming cells, $n = 3$ donors, three technical replicates each, mean ± SD, nonlinear regression (curve fit). (**G**) Coculture of NT, TCR$^+$, or TCR8$^+$ CD4$^+$ (red bars) or CD8$^+$ (black bars) T cells with BV173 leukemia cells (HLA-A2*02:01$^+$survivin$^+$); E:T ratio 1:5, residual BV173 cells quantified on day 3, $n = 7$. (**H**) Coculture of NT, TCR$^+$, or TCR8$^+$CD4$^+$ (left) or CD8$^+$ (right) T cells with wild-type (WT) BV173 (solid bars) or β2-microglobulin knockout (B2M-KO) BV173 cells (open bars); E:T ratio 1:5, residual BV173 cells quantified on day 3, $n = 3$. Mean ± SD, ***$P < 0.001$ and ****$P < 0.0001$. t test on log-transformed data.

up-regulated genes were shared between TCR8$^+$CD4$^+$ and TCR8$^+$CD8$^+$ ($n = 60$) than between TCR8$^+$CD4$^+$ and TCR$^+$CD8$^+$ T cells ($n = 24$) or between TCR8$^+$CD8$^+$ and TCR$^+$CD8$^+$ T cells ($n = 10$). Among the shared genes in TCR8$^+$CD4$^+$ and TCR8$^+$CD8$^+$ T cells, several genes were associated to the T_N and T_{CM} phenotype (e.g., *IL7R*, *CXCR4*, and *FOXP1*) as well as costimulation (*CD2* and *CD82*). Only 27 genes were shared by all three cocultured T cell types (Fig. 2 E and table S2).

These results demonstrate that single-cell transcriptomics identified distinct cellular subpopulations in each sample type analyzed and gave insight into the population dynamics during T cell manufacturing and tumor exposure. Major lineage- and transgene-dependent changes were detected upon coculture, and cocultured TCR8$^+$CD4$^+$ T cells were most unique.

Cocultured CD4$^+$ T cells better sustain their replicative capacity, and TCR8 expression promotes a less differentiated phenotype

Next, we used published gene sets (table S3) to deeply characterize the T cell proliferation and differentiation states in each condition (Fig. 3) (*30*). As described above, replicating cells were identified in expanded as well as in cocultured CD4$^+$ and CD8$^+$ T cells (Figs. 2C and 3, A to C, and fig. S3). Cocultured TCR8$^+$CD4$^+$ T cells sustained high expression of replicating genes and maintained the replicating population size, in contrast to TCR$^+$ or TCR8$^+$CD8$^+$ T cells that showed a sharp decrease in replication (Fig. 3, B and C). We then investigated expression of T_N, T_{CM}, effector memory (T_{EM}), and effector (T_{EFF}) gene signatures (*30*). Hierarchical clustering was used to divide each T cell condition into four clusters that were assigned the differentiation status of T_N, T_{CM}, T_{EM}, and T_{EFF} cells, and color coded in the t-SNE plot (Fig. 3D and fig. S6). We found that TCR8$^+$CD4$^+$ T cells retained a less differentiated gene expression profile than the TCR$^+$CD8$^+$ or TCR8$^+$CD8$^+$ T cells (Fig. 3, D and E, bars). Independent two-marker–based FACS validation (CD62L and CD45RO) confirmed the distribution of the subpopulations in bulk T cells (Fig. 3E, lines with dots). Fresh cells contained mostly T_N and T_{CM} cells and small populations of T_{EM} and T_{EFF} cells. Expanded TCR$^+$ and TCR8$^+$CD4$^+$ T cells were significantly enriched in T_{CM} cells when compared with expanded TCR$^+$ and TCR8$^+$CD8$^+$

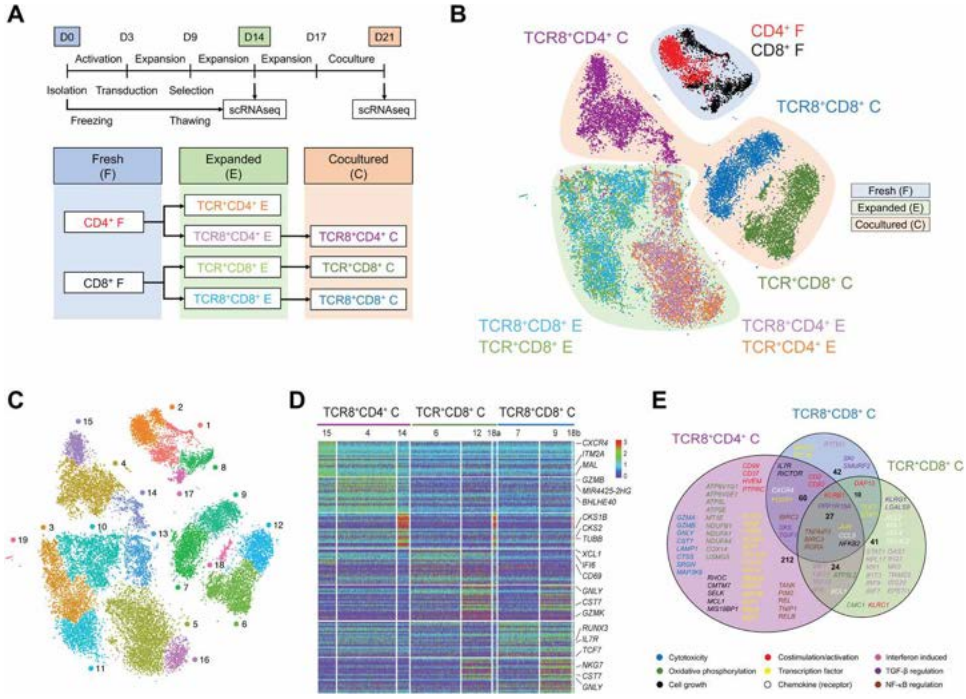

Fig. 2. Single-cell transcriptomics reveals distinct T cell subpopulations. (**A**) Schematic overview of experimental setup and corresponding groups. (**B**) t-SNE plot of all 25,474 cells analyzed, color code indicates sample origin, and each dot represents one cell. (**C**) t-SNE plot of all cells separated into 19 distinct clusters by k-nearest neighbor clustering analysis; each cluster is color coded. (**D**) Heat map showing the top 20 DE genes of each cluster for all cocultured samples with selected genes identified on the right. Cluster 18 contains cocultured TCR$^+$CD8$^+$ and cocultured TCR8$^+$CD8$^+$ cells, depicted as clusters 18a and 18b on the heat map. (**E**) Venn diagram of DE genes (0.25 log fold change) up-regulated from expanded to cocultured state. Distinct or shared representative genes from each cocultured sample are indicated and color coded by biological function.

T cells ($P = 0.0005$ and $P = 0.0003$, respectively; Fig. 3E). Expanded CD8$^+$ T cells were characterized by higher proportions of T_{EM} (TCR$^+$, $P = 0.003$; TCR8$^+$, $P = 0.01$) and T_{EFF} (TCR$^+$, $P < 0.0001$; TCR8$^+$, $P = 0.0002$) when compared with expanded CD4$^+$ T cells. Cocultured TCR8$^+$CD4$^+$ T cells better preserved a less differentiated phenotype (T_N and T_{CM}) transcriptionally compared with cocultured TCR$^+$CD8$^+$ or TCR8$^+$CD8$^+$ T cells, which was confirmed by FACS for T_{CM} ($P < 0.0001$ and $P = 0.006$, respectively; Fig. 3E). In addition, we observed significantly less T_{EFF} cells in cocultured TCR8$^+$CD4$^+$ compared with TCR$^+$CD8$^+$ and TCR8$^+$CD8$^+$ T cells ($P = 0.0003$ and $P = 0.006$, respectively; Fig. 3E). We also detected a TCR8 transgene–mediated effect in CD8$^+$ T cells with significantly increased T_{CM} and decreased T_{EFF} populations upon coculture ($P = 0.04$ and $P = 0.03$, respectively; Fig. 3E). While this effect was not confirmed in the hierarchical clustering analysis, we detected a TCR8-dependent increase in gene expression of important T_N/T_{CM}-associated genes such as *TCF7*, *IL7R*, *CCR7*, and *CXCR4* (Fig. 3F). Overall, TCR8$^+$CD4$^+$ T cells were characterized by a bigger proliferating population and simultaneous preservation of a less differentiated phenotype compared with CD8$^+$ T cells, suggesting that TCR8$^+$CD4$^+$ T cells have a higher potential for long-term persistence and antitumor function in vivo.

TCR8 promotes cytotoxicity and costimulation in the absence of exhaustion in CD4$^+$ T cells

On the basis of the analysis of gene DE (Fig. 2, D and E), we found up-regulation of cytotoxic pathways in cocultured TCR8$^+$CD4$^+$ T cells, some of them even to higher levels compared with TCR$^+$CD8$^+$ or TCR8$^+$CD8$^+$ T cells (e.g., *GZMA* and *GZMB*). A manually curated gene signature was used to visualize cytotoxic cells (Fig. 4A and table S3). In cocultured T cells, they colocalized with clusters 4, 9, and 12 identified in Fig. 2C, as well as T_{EM} and T_{EFF} cell clusters shown in Fig. 3D. Among the top up-regulated genes were *GZMA* and *GZMB* (Fig. 2D), both of which were visualized by t-SNE (Fig. 4B, top) and validated by FACS (Fig. 4B, bottom). Following an increase in *GZMB* mRNA levels, GZMB protein levels increased significantly from expanded to cocultured state in TCR8$^+$CD4$^+$ T cells ($P = 0.002$;; Fig. 4B, left). In contrast, *GZMB* gene expression was reduced in TCR$^+$CD8$^+$ and TCR8$^+$CD8$^+$ T cells upon coculture, and a significant reduction in GZMB protein expression was observed in TCR$^+$CD8$^+$ T cells ($P = 0.002$; Fig. 4B, left). Similar results were obtained for *GZMA* mRNA expression, but intracellular protein levels of GZMA remained high in all cocultured T cells (Fig. 4B, right). While a significant decrease in GZMA was observed in TCR8$^+$CD4$^+$ T cells during coculture ($P = 0.004$; Fig. 4B, right), their overall GZMA levels were similar to cocultured TCR$^+$ and TCR8$^+$CD8$^+$ T cells. To corroborate our findings, we performed a single-cell killing stress test using high-throughput time-lapse imaging microscopy in nanowell grids (TIMING) (*31*, *32*). The time needed to establish a stable conjugation with the target (t_{Seek}), the total duration of conjugation ($t_{Contact}$), and the time between first contact and tumor cell apoptosis (t_{Death}) were measured over 9 hours (Fig. 4C). CD8$^+$ T cells were efficient at finding their target and establishing a stable conjugation. TCR$^+$CD8$^+$ T cells were more

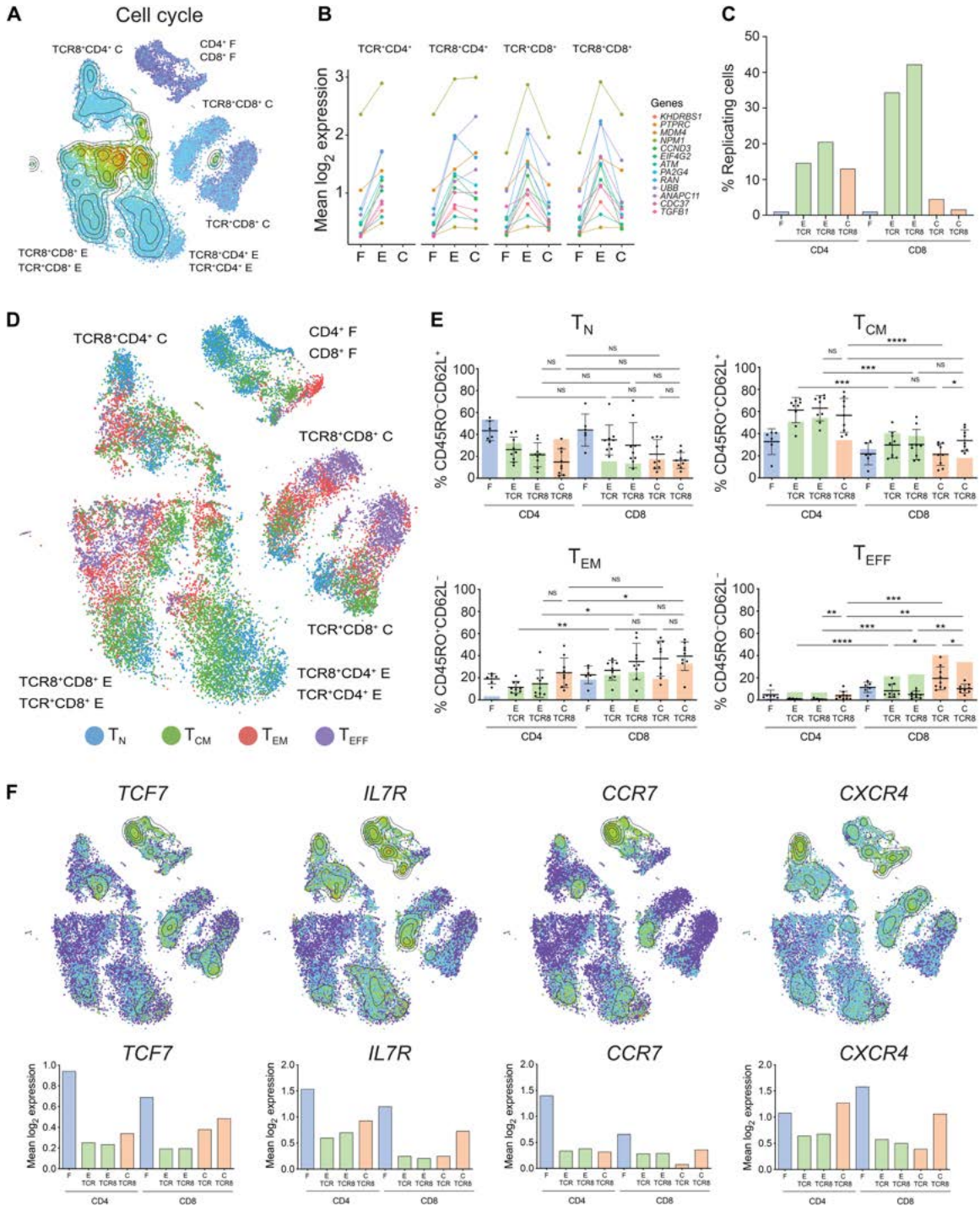

Fig. 3. Sustained proliferative capacity and preservation of a less differentiated phenotype in cocultured TCR8$^+$CD4$^+$ T cells. (**A**) t-SNE plot of cell cycle–associated genes (GO_0007049) revealing location of proliferating cells in each sample. (**B**) Mean expression pseudo time course of cell cycle–related genes for each sample. Pseudo time points represent fresh (F), expanded (E), and cocultured (C) conditions. (**C**) Bar plot representing proportion of replicating T cells per sample. The replicating cells are defined by their association to clusters 10, 13, 14, and 18. (**D**) t-SNE plot of T_N, T_{CM}, T_{EM}, and T_{EFF} cells identified by hierarchical clustering. Each dot represents one cell color coded by differentiation status. (**E**) Combined plot overlaying % cells for each subset by t-SNE (bars) and two-marker–based FACS validation (line with dots, CD62L and CD45RO, $n = 9$ independent donors, mean ± SD and individual values, Mann-Whitney U test). *$P < 0.05$, **$P < 0.01$, ***$P < 0.001$, and ****$P < 0.0001$. (**F**) t-SNE plot (top) and corresponding bar plot (bottom) showing mean gene expression of representative T_N/T_{CM} markers *TCF7*, *IL7R*, *CCR7*, and *CXCR4*.

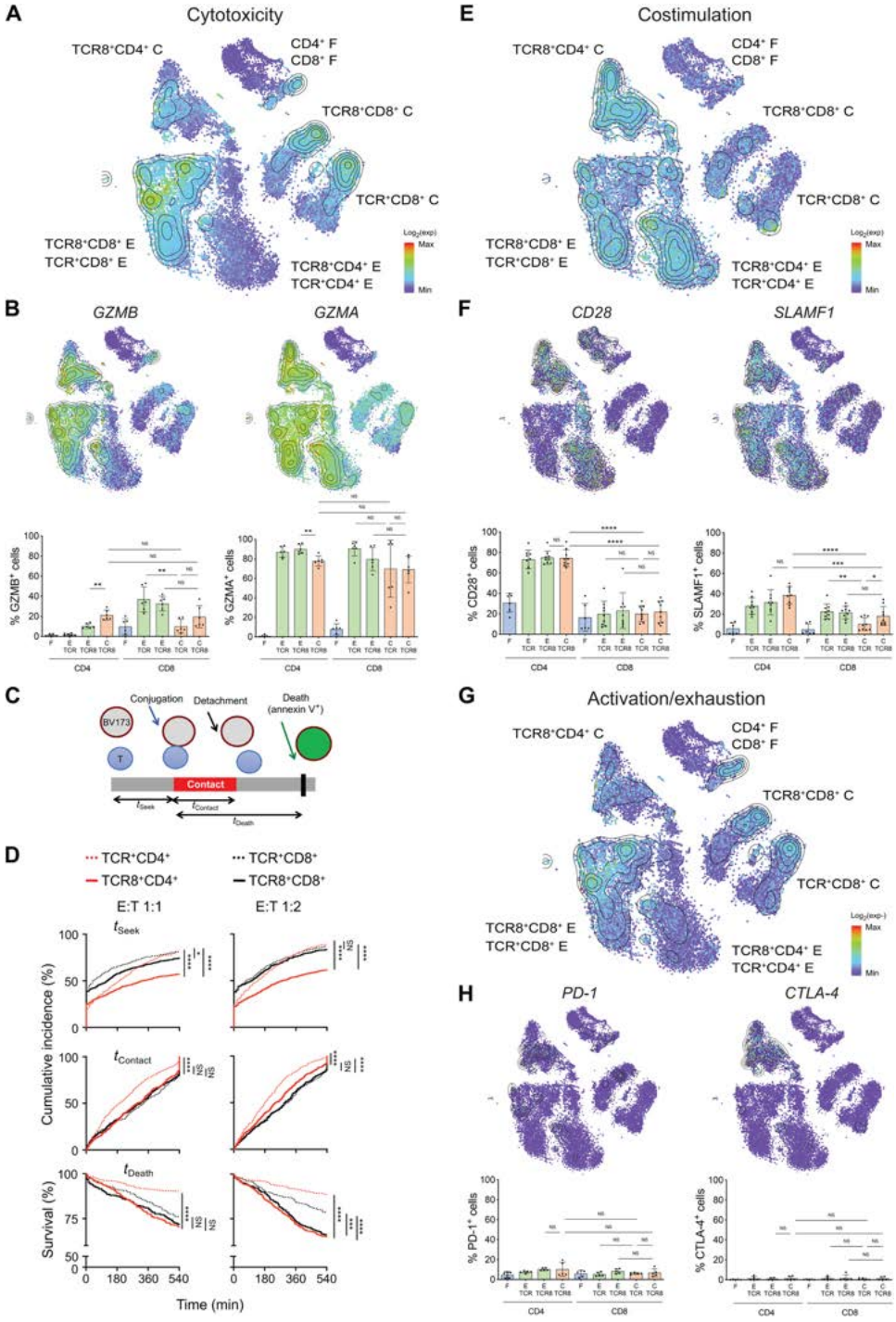

Fig. 4. TCR8 promotes cytotoxicity and costimulation in TCR8$^+$CD4$^+$ T cells in the absence of exceeding activation/exhaustion. (**A**) t-SNE plot of cytotoxicity-related genes (list of genes provided in table S3). (**B**) t-SNE plot of *GZMB* and *GZMA* (top) and intracellular FACS validation of T cells stimulated with BV173 cells (bottom, $n = 6$ independent donors, mean ± SD and individual values, Mann-Whitney *U* test). $^{**}P < 0.01$. (**C**) Single-cell quantification of interaction kinetics between T cells and target cells by TIMING assay. t_{Seek}, time to first encounter of effector and target cell; $t_{Contact}$, time of conjugation between effector and target cell; t_{Death}, time from first contact to target cell apoptosis. (**D**) Cumulative incidence of a single T cell in finding (t_{Seek}) one (left, E:T 1:1) or two (right, E:T 1:2) target cells (top row), in forming a stable synapse with the target ($t_{Contact}$, middle row), or in killing the target (t_{Death}). TCR$^+$CD4$^+$ T cells (red dotted lines), TCR8$^+$CD4$^+$ T cells (red solid lines), TCR$^+$CD8$^+$ T cells (black dotted lines), and TCR8$^+$CD8$^+$ T cells (black solid lines). $^*P < 0.05$, $^{**}P < 0.01$, $^{***}P < 0.001$, and $^{****}P < 0.0001$, log-rank test. (**E**) t-SNE plot of costimulation-related genes (list of genes provided in table S3). (**F**) t-SNE plot of *CD28* and *SLAMF1* (top) and FACS validation (bottom, $n = 6$ to 9 independent donors, mean ± SD and individual values, Mann-Whitney *U* test). $^*P < 0.05$, $^{***}P < 0.001$, and $^{****}P < 0.0001$. (**G**) t-SNE plot of activation/exhaustion related-genes (list of genes provided in table S3). (**H**) t-SNE plot of *PD-1* and CTLA-4 (top) and FACS validation (bottom, $n = 5$ independent donors, mean ± SD and individual values, Mann-Whitney *U* test).

efficient than TCR8$^+$CD8$^+$ T cells at finding targets at the E:T 1:1 (Fig. 4D top, t_{Seek} TCR$^+$CD8$^+$ versus TCR8$^+$CD8$^+$, $P = 0.01$) but established equally stable contacts (Fig. 4D, middle, $t_{Contact}$, P = NS). Their killing capacity was equivalent at E:T 1:1 single T cell and single target cell per well (Fig. 4D, bottom left, P = NS); however, sequential killing capacity was significantly enhanced in TCR8$^+$CD8$^+$ T cells at E:T 1:2 (single T cell and two target cells per well; Fig. 4D, bottom right, $P = 0.0002$). As expected, TCR$^+$CD4$^+$ T cells were not able to form stable conjugates and kill the target cells, despite the fact that they were actively seeking targets and found contacts (Fig. 4D, t_{Seek} and $t_{Contact}$, TCR$^+$CD4$^+$ versus TCR8$^+$CD4$^+$, $P < 0.0001$). However, TCR8$^+$CD4$^+$ T cells efficiently killed their targets. At E:T 1:1, TCR8$^+$CD4$^+$ T cells found, conjugated to, and killed their target as efficiently as TCR$^+$CD8$^+$ or TCR8$^+$CD8$^+$ T cells (Fig. 4D, P = NS). At E:T 1:2, TCR8$^+$CD4$^+$ T cells killed as efficiently as TCR8$^+$CD8$^+$ T cells (Fig. 4D, bottom right, P = NS), and killed better than TCR$^+$CD8$^+$ T cells (Fig. 4D, bottom right, $P < 0.0001$).

Next, we analyzed costimulatory and activation/exhaustion-related genes (table S3) (*33*) and found enhanced expression of costimulatory genes in cocultured TCR8$^+$CD4$^+$ T cells (Fig. 4E). For example, high *CD28* and signaling lymphocytic activation molecule family 1 (*SLAMF1*) gene expression correlated with high protein expression in CD4$^+$ T cells, and both remained stably expressed after coculture (Fig. 4F). CD28 protein expression was significantly higher in cocultured TCR8$^+$CD4$^+$ compared with TCR$^+$CD8$^+$ and TCR8$^+$CD8$^+$ T cells (Fig. 4F, left, $P < 0.0001$ and $P < 0.0001$, respectively). SLAMF1 expression was also significantly higher in cocultured TCR8$^+$CD4$^+$ T cells compared with cocultured TCR$^+$ and TCR8$^+$CD8$^+$ T cells (Fig. 4F, right, $P < 0.0001$ and $P = 0.0008$, respectively). A sharp decrease in SLAMF1 expression from expansion to coculture was observed in TCR$^+$CD8$^+$ T cells ($P = 0.003$) but not in TCR8$^+$CD8$^+$ T cells, suggesting a TCR8 transgene–mediated effect on SLAMF1 expression. Other costimulatory markers were also validated by FACS (CD40L, CD70, and HVEM) and highlight our finding of enhanced costimulatory marker expression in cocultured TCR8$^+$CD4$^+$ T cells (fig. S5B). Transcription of genes associated with T cell exhaustion or recent activation was increased in expanded and cocultured CD8$^+$ compared with CD4$^+$ T cells (Fig. 4G) and colocalized with cytotoxicity-associated genes (Fig. 4A) as well as T_{EM} and T_{EFF} cells (Fig. 3D). Experimental validation for PD-1 and CTLA-4 expression by FACS showed an overall low expression in all populations analyzed (Fig. 4H, bottom).

These combined transcriptional and functional single-cell data established that expression of TCR8 enabled the conversion of CD4$^+$ T cells into efficient sequential killers and that sustained expression of *GZMB* plays an important role in the antitumor activity of TCR8$^+$CD4$^+$ T cells. The combination of high costimulatory and low T cell exhaustion/activation–related genes in TCR8$^+$CD4$^+$ T cells favors an increased capacity for long-term persistence and antitumor function compared with engineered CD8$^+$ T cells.

Cocultured TCR8$^+$CD4$^+$ T cells heavily rely on OXPHOS and have higher mitochondrial activity compared with cocultured CD8$^+$ T cells

OXPHOS was the major metabolic pathway highly up-regulated in cocultured TCR8$^+$CD4$^+$ T cells (Fig. 2E). As expected, all expanded activated T cells augmented global metabolism, and thus engaged heavily in OXPHOS (Fig. 5, A and B), glycolysis (Fig. 5, D and E), and fatty acid oxidation (FAO; Fig. 5, F and G). High expression of OXPHOS, glycolysis, and FAO genes was retained exclusively in TCR8$^+$ CD4$^+$ T cells upon coculture and declined sharply in both cocultured CD8$^+$ samples (Fig. 5, B, E, and G). To confirm that increased metabolic gene expression in CD4$^+$ T cells correlated with higher mitochondrial activity, a key feature leading to superior proliferative capacity and antitumor responses of engineered T cells (*34*), we investigated mitochondrial mass by FACS (*35*). A significant reduction in mitochondrial mass was observed in CD8$^+$ T cells after expansion to coculture ($P = 0.0002$; Fig. 5C), in contrast to CD4$^+$ T cells. TCR8$^+$CD8$^+$ T cells preserved a significantly higher mitochondrial mass compared with TCR$^+$CD8$^+$ T cells ($P = 0.03$; Fig. 5C), suggesting a TCR8 transgene–mediated impact on mitochondrial content. Mitochondrial mass in cocultured CD4$^+$ T cells was significantly higher than in cocultured TCR$^+$CD8$^+$ and TCR8$^+$CD8$^+$ T cells ($P = 0.0002$ and $P = 0.015$, respectively; Fig. 5C). Our results suggest that TCR8$^+$CD4$^+$ T cells sustain a higher metabolic activity accompanied by an increased mitochondrial content and a strong preference for OXPHOS.

TCR8$^+$CD4$^+$ T cells efficiently kill and expand under stress conditions in vitro and in vivo

To perform an in vitro stress test with high tumor burden, we challenged CD4$^+$ and CD8$^+$ T cells transduced with TCR, TCR8, or non-transduced (NT) controls up to four times with fresh BV173 leukemia cells (Fig. 6, A and B). We found a significantly increased sequential tumor killing capacity for TCR8$^+$CD8$^+$ compared with TCR$^+$CD8$^+$ T cells ($P = 0.04$; Fig. 6B, top right). Again, CD4$^+$ T cells only killed when transduced with TCR8 but not with TCR alone ($P < 0.0001$; Fig. 6B, top left). TCR8$^+$CD4$^+$ T cells were better sequential killers than TCR$^+$CD8$^+$ T cells ($P = 0.01$) but as efficient as TCR8$^+$CD8$^+$ T cells (P = NS). TCR8$^+$CD4$^+$ T cells expanded significantly better than TCR$^+$CD8$^+$ T cells ($P = 0.002$) and TCR8$^+$CD8$^+$ T cells ($P = 0.015$) upon tumor challenge (Fig. 6B, bottom, dotted lines). To further characterize the cytotoxic phenotype, we examined cytokine production 1 day after initial plating (D1) and after the third tumor challenge (D10). The cytokine production profile was not significantly altered in TCR$^+$ versus TCR8$^+$CD8$^+$ T cells. However, CD4$^+$ T cells produced a T_H1-predominant cytotoxic cytokine pattern only when transduced with TCR8. TCR8$^+$CD4$^+$ T cells secreted multiple cytokines or lytic granules including IFN-γ, tumor necrosis factor–α, perforin, or granzyme B, with levels comparable to TCR$^+$ or TCR8$^+$CD8$^+$ T cells (Fig. 6C). These findings were corroborated by intracellular cytokine staining after tumor challenge (fig. S7A). Intracellular cytokines and cytotoxic protein levels correlated with CD45RO expression in accordance with the transcriptional overlap of T_{EM} and cytotoxic populations based on scRNAseq data (fig. S7B and Figs. 3D and 4A). Despite down-regulation of CD62L resulting from the intracellular staining procedure, we detected an inverse correlation of CD62L$^+$ cells with cytokine and cytotoxic protein production. Next, we tested the in vivo antitumor function of transgenic T cells in our leukemia xenograft model using NSG mice engrafted with BV173.ffLuc leukemia (Fig. 6D) (*23*). We observed significant leukemia control in mice treated with TCR$^+$CD8$^+$ T cells compared with NT controls and further enhancement in mice treated with TCR8$^+$CD8$^+$ T cells (NT versus TCR, $P = 0.0002$; NT versus TCR8, $P < 0.0001$; TCR versus TCR8, $P = 0.01$; Fig. 6E). TCR8$^+$CD4$^+$ T cells also significantly delayed leukemia progression compared with TCR$^+$CD4$^+$ T cells ($P = 0.001$; Fig. 6F), and TCR8$^+$CD4$^+$ T cells significantly better controlled tumor

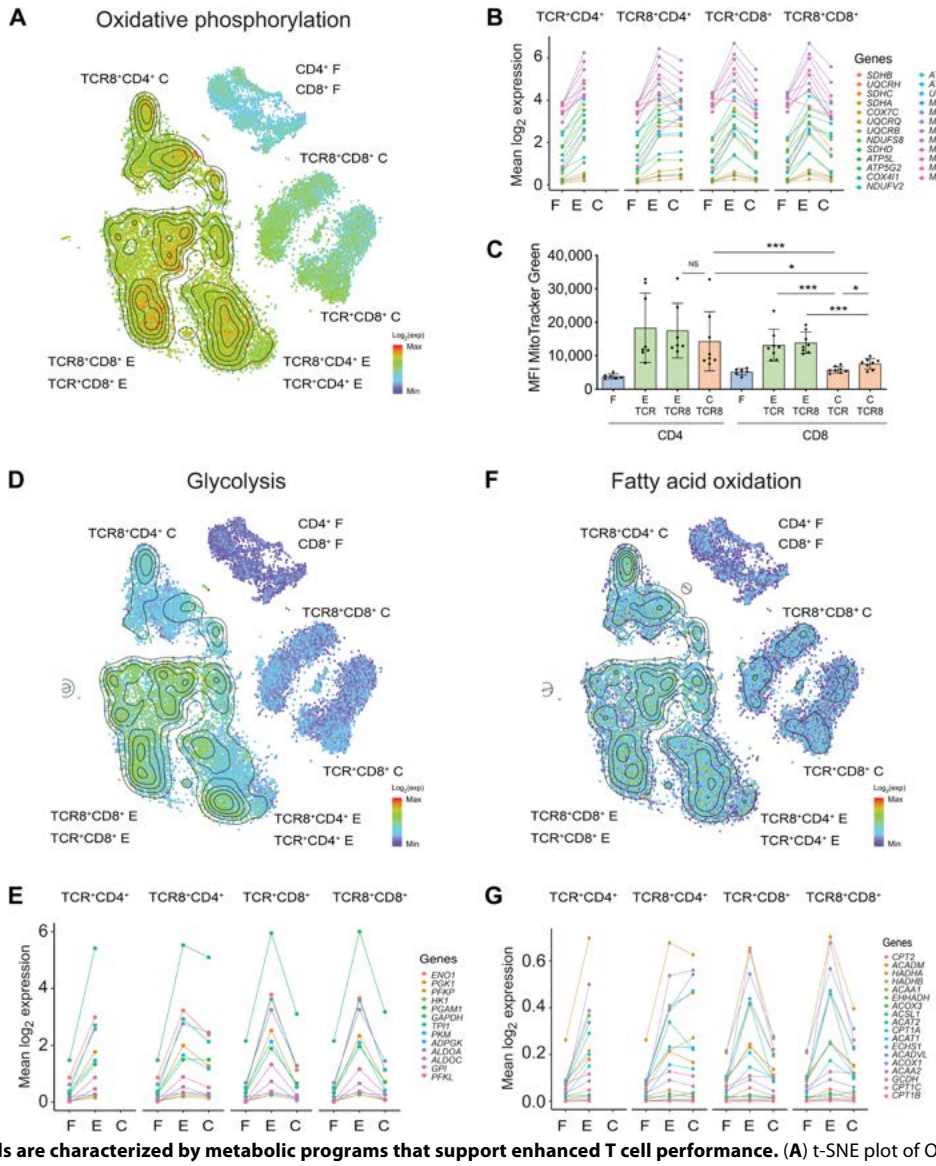

Fig. 5. TCR8$^+$CD4$^+$ T cells are characterized by metabolic programs that support enhanced T cell performance. (**A**) t-SNE plot of OXPHOS-related genes [HUGO Gene Nomenclature Committee (HGNC) database group 639, four to five representative genes per complex]. (**B**) Mean expression pseudo time course of representative OXPHOS genes. (**C**) Absolute MFI values for mitochondrial membrane potential (left) and mass (right) determined by FACS ($n = 7$ to 8 independent donors, mean ± SD and individual values, Mann-Whitney U test). *$P < 0.05$ and ***$P < 0.001$. (**D**) t-SNE plot of glycolysis-related genes (KEGG database). (**E**) Mean expression pseudo time course of indicated genes. (**F**) t-SNE plot of FAO-related genes (KEGG database). (**G**) Mean expression pseudo time course of indicated genes.

growth compared with TCR8$^+$CD8$^+$ T cells ($P = 0.01$). Thus, TCR8 expression enhances antitumor function of CD8$^+$ T cells, confers cytotoxicity to CD4$^+$ T cells, and TCR8$^+$CD4$^+$ T cells have the overall best antitumor activity in the mouse model in vivo.

DISCUSSION

With the goal of rigorously investigating the functional and transcriptomic effects in different types of TCR-engineered therapeutic human T cells, we explored population and single-cell functional and transcriptomic properties of purified CD4$^+$ and CD8$^+$ T cells. The T cells were redirected to a class I–restricted TAA epitope with a survivin-specific TCR alone (TCR) (*23*) or in combination with the CD8αβ coreceptor (TCR8). The three main questions we addressed were (i) whether TCR8-redirected CD4$^+$ and CD8$^+$ T cells were functionally comparable (bulk and single-cell assays), (ii) whether single-cell transcriptomics could identify unique features in TCR8-redirected CD4$^+$ and CD8$^+$ T cells after expansion and coculture with tumor targets, and (iii) whether redirection with TCR or TCR8 modified the single-cell cytotoxic activity or transcriptome of cocultured CD8$^+$ T cells.

We validated our experimental system by showing that CD4$^+$ T cells are successfully redirected to the targeted survivin epitope by TCR8 transduction and that these redirected TCR8$^+$CD4$^+$ T cells killed HLA-A*0201$^+$survivin$^+$ BV173 leukemia target cells in a class I–restricted manner, corroborating previous studies that used other TCRs (*1*–*6*). At the bulk level, the redirected TCR8$^+$CD4$^+$ T cells were functionally comparable to TCR$^+$ or TCR8$^+$CD8$^+$ T cells in vitro.

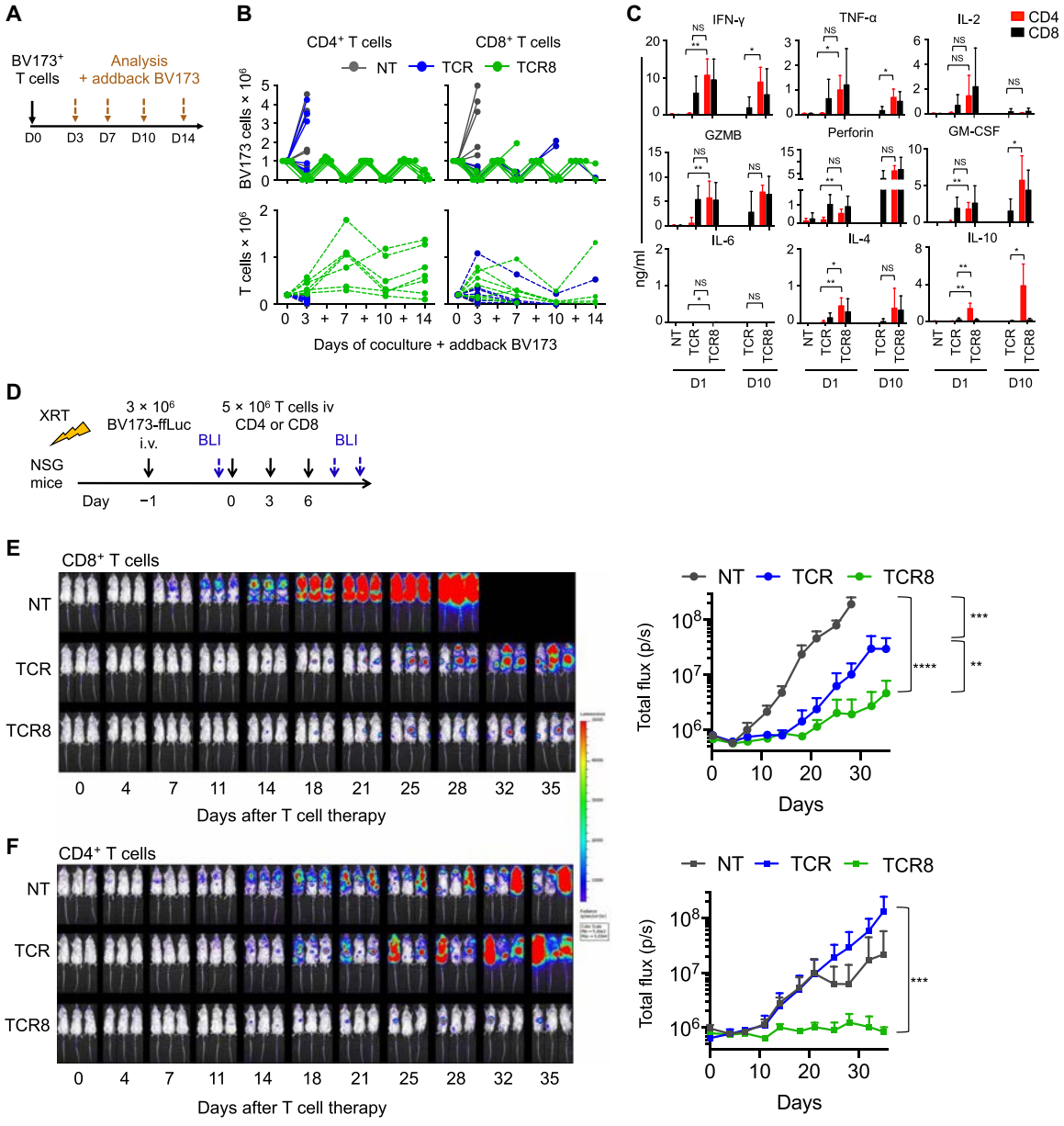

Fig. 6. TCR8$^+$CD4$^+$ T cells efficiently kill and expand under stress conditions in vitro and in vivo. (**A**) Experimental setup of bulk sequential coculture stress test. (**B**) Sequential cocultures of CD4$^+$ (left) or CD8$^+$ (right) T cells. Quantification of tumor (top) and T cells (bottom) over time, with tumor cell rechallenge (+), $n = 7$. Number of tumor cell killings by condition: CD4$^+$ T cells: NT 0 ± 0, TCR$^+$ 0 ± 0, TCR8$^+$ 3.2 ± 0.5; CD8$^+$ T cells: NT 0 ± 0, TCR$^+$ 1.3 ± 1.1, TCR8$^+$ 2 ± 1.4. TCR$^+$CD8$^+$ versus TCR8$^+$CD8$^+$ T cells: $P = 0.04$; TCR8$^+$CD4$^+$ versus TCR$^+$CD8$^+$ T cells: $P = 0.01$; TCR8$^+$CD4$^+$ versus TCR8$^+$CD8$^+$ T cells: P = NS, t test. T cell expansion: TCR$^+$CD8$^+$ versus TCR8$^+$CD8$^+$: P = NS; TCR8$^+$CD4$^+$ versus TCR$^+$CD8$^+$: $P = 0.002$; TCR8$^+$CD4$^+$ versus TCR8$^+$CD8$^+$, $P = 0.015$, t test on log AUC. (**C**) Cytokine quantification in coculture supernatants 24 hours after first tumor challenge (D1) and 24 hours after third tumor challenge (D10), $n = 6$. Mean ± SD, *$P < 0.05$ and **$P < 0.01$. (**D**) Experimental setup mouse xenograft experiment. XRT, radiation; BLI, bioluminescence imaging; iv, intravenously. (**E** and **F**) BLI results from mice treated with (E) CD8$^+$ T cells or (F) CD4$^+$ T cells. BLI pictures show three representative mice per group, color scale 5 × 10^3 to 5 ×10^4 p/sec/cm^2/sr (left) and summary of total flux (right). Nontransduced (NT) control T cells ($n = 5$, gray), TCR$^+$ T cells ($n = 5$, blue), TCR8$^+$ T cells ($n = 5$, green). Mean ± SD. **$P < 0.01$, ***$P < 0.001$, and ****$P < 0.0001$. t test on log AUC, day 28 for CD8$^+$, day 35 for CD4$^+$ T cells.

However, the single-cell killing assay in vitro as well as the mouse xenograft model in vivo revealed a significant benefit of the TCR8 transgene compared with TCR alone in CD8$^+$ T cells, mediating enhanced sequential killing capacity in vitro and better leukemia control in vivo. Most likely, the imbalance between available endogenous CD8αβ and transgenic TCR molecules in TCR$^+$CD8$^+$ T cells represents the limiting factor for efficient immunological synapse formation and antitumor function, as retroviral transduction results in expression of supraphysiologic copy numbers of the inserted gene(s) (*36*, *37*). A similar effect has been previously reported upon transgenic expression of the four CD3 chains in TCR transgenic T cells (*38*). These findings indicate that forced expression of TCR8 not only is a strategy to redirect CD4$^+$ T cells against class I epitopes but also significantly enhances transgenic CD8$^+$ T cell function.

Using scRNAseq, we identified various distinct transcriptionally defined T cell subpopulations. T cell lineage origin ($CD4^+$ or $CD8^+$) and cell state (fresh, expanded, or cocultured) had the strongest effects on spatial distribution of the cells in the t-SNE analysis. We focused our investigations on the changes occurring between the expanded and cocultured states, since we aimed to identify the DE genes and pathways in engineered T cells that are associated with enhanced T cell performance (sequential tumor killing, sustained T cell expansion, and enhanced in vivo cytotoxicity). We found that the most marked transcriptional changes occurred in $TCR8^+CD4^+$ T cells upon coculture. Sustained up-regulation of several pathways known to be crucial for long-term function of tumor-redirected engineered T cells were uncovered, such as cytotoxicity, costimulation, OXPHOS, cell cycle, and proliferation, as well as a greater diversity of expressed transcription factors. Specifically, these pathways were initially up-regulated in both expanded $CD4^+$ and $CD8^+$ T cells, but only in cocultured $TCR8^+CD4^+$ T cells was their expression sustained. In addition, exhaustion-associated genes were lower in $CD4^+$ compared with $CD8^+$ T cell conditions. The summary of these findings points toward a complex interplay between pathways that overall lead to enhanced T cell performance.

Several associations between some of these pathways are well described in T cells. For example, costimulation through CD28 has been shown to be a key driver for enhancing glucose metabolism and mitochondrial activity in T cells, leading to formation of a functional memory T cell pool (*39*, *40*). We found high *CD28* mRNA and CD28 protein expression levels in $CD4^+$ T cells, with a concomitant high expression of glycolysis-related genes and mitochondrial mass that was retained during coculture. The mitochondrial surplus present in human $CD4^+$ T cells has previously been associated with resistance to cellular senescence compared with $CD8^+$ T cells and may, therefore, contribute to better leukemia killing and proliferation of $TCR8^+CD4^+$ T cells (*41*). In addition, OXPHOS, a major metabolic pathway in long-term persisting memory T cells (*42*), was highly activated in $TCR8^+CD4^+$ T cells, which also preserved more cells with T_{CM} phenotype by gene expression and protein levels compared with $CD8^+$ T cells. A previous report has shown that CAR T cells signaling through the 41BB costimulatory endodomain predominantly use OXPHOS over glycolysis and are characterized by enhanced T cell proliferation and persistence (*34*). In addition, $TCR8^+CD4^+$ T cells retained a larger replicating cell population than $CD8^+$ T cells and sustained expression of cell cycle genes, in line with the observation that $TCR8^+CD4^+$ T cells expanded better during sequential tumor challenges. Because all these beneficial properties can be categorized as CD4 lineage–related effects, a direct impact of CD4 coreceptor signaling must also be considered. Both the CD4 and CD8 coreceptors are associated with LCK and mediate the activation of early TCR signaling. The amount of LCK associated with the CD4 coreceptor is between 10 and 20 times higher than LCK bound to the CD8 coreceptor (*43*). Thus, $TCR8^+CD4^+$ T cells may benefit from this higher availability of LCK during early TCR signaling events more than engineered $CD8^+$ T cells. We also observed that $TCR8^+CD4^+$ cells produced low levels of interleukin-4 (IL-4) and IL-10 upon coculture, indicating a T_H1/T_H2 hybrid phenotype. These findings are in line with a recent paper evaluating the single-cell transcriptome and cytokine production profile of $CD4^+$ and $CD8^+$ human T cells engineered with a third-generation CD19 CAR (*44*). In our TCR system, the T_H1 phenotype and function predominated, with a minor T_H2 population that did not reduce antitumor function in vitro or in vivo. High expression of costimulatory molecules (CD28, SLAMF1, and CD70) combined with enhanced pLCK signaling upon target recognition may override the potentially inhibitory effects of IL-10. Together, these findings suggest that $TCR8^+CD4^+$ T cells are characterized by several lineage-specific advantages including high expression of costimulatory molecules, higher mitochondrial content, and an overall enhanced metabolic competitiveness during coculture, which enables better proliferation and functionality in the tumor microenvironment.

Transgene type (TCR or TCR8) only segregated $CD8^+$ T cell populations upon coculture. The most marked common feature in cocultured $TCR8^+CD4^+$ and $TCR8^+CD8^+$ compared with TCR^+CD8^+ T cells was the preservation of a less differentiated phenotype by expression of T_N-and T_{CM}-associated genes that we confirmed by FACS. A significantly higher proportion of T_{CM} cells were detected in cocultured $TCR8^+CD4^+$ and $TCR8^+CD8^+$ compared with TCR^+CD8^+ T cells. It has previously been shown that T_N- or T_{CM}-derived $CD8^+$ T cells outperform more differentiated effector T cells upon adoptive transfer (*45*–*47*), and this phenotype is desired for adoptive T cell therapy (*48*). A larger population of less differentiated T cells in the $TCR8^+CD4^+$ or $TCR8^+CD8^+$ conditions may contribute to the observed enhanced antitumor function in vitro and in vivo. Sustained expression of CXCR4 on engineered T cells could be of particular interest when targeting hematologic malignancies, because CXCR4 mediates T cell homing to the bone marrow microenvironment (*49*). TCR8 expression in $CD8^+$ T cells also leads to an increased SLAMF1 expression and a higher mitochondrial mass compared with TCR^+CD8^+ T cells. Thus, additional CD8αβ coreceptor signaling may support the retention of some costimulatory molecules and mitochondrial homeostasis during coculture.

$CD4^+$ T cells exert a great variety of functions in orchestrating efficient immune responses against infections and cancer, and their interplay with $CD8^+$ T cells is of crucial importance (*19*, *50*), as recently demonstrated by the adoptive transfer of $CD4^+$ T_H1 tumor-infiltrating lymphocytes targeting tumor neoantigens, or by the infusion of CD19-CAR T cells with a defined ratio of CD4:CD8 T cells (*22*, *51*, *52*). In a preclinical study evaluating the antitumor function of IL-13Rα2 CAR T cells against glioblastoma, $CD4^+$ CAR T cells alone were more potent than $CD8^+$ CAR T cells alone or mixed populations at defined CD4:CD8 ratios (*53*). Thus, functional $CD4^+$ T cells should likely be incorporated into TCR transgenic T cell products for adoptive transfer, as $CD4^+$ T cells can greatly contribute to tumor control and $CD8^+$ T cell persistence after adoptive transfer. It needs to be evaluated whether purified $CD4^+$ T cells or a more rigidly formulated product with a specific CD4:CD8 ratio is preferable for TCR T cell therapy. The data from the CAR T cell field indicate that tumor histology probably also plays a role in determining the best formulation of the infusion product. Healthy donor or patient origin of the starting material may also influence the overall functional outcome of the final product.

Overall, transgenic coexpression of the CD8αβ coreceptor had beneficial effects on the function of $TCR8^+CD8^+$ and $TCR8^+CD4^+$ T cells in vitro and in vivo. $TCR8^+CD4^+$ T cells are polyfunctional hybrid T cells with simultaneous cytotoxic effector functions and preserve native $CD4^+$ T cell functions at the single-cell level. We uncovered previously unknown profound transcriptional changes that occur in $TCR8^+CD4^+$ T cells upon tumor challenge. The identified pathways are known to play crucial roles in the long-term persistence and antitumor function of engineered T cells in the tumor

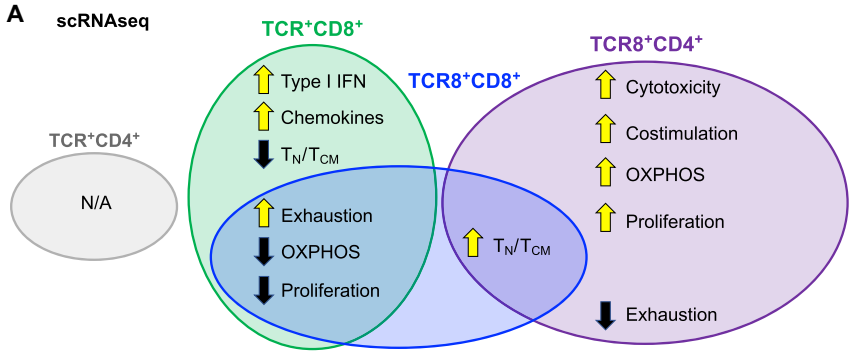

B

Functional assay	TCR+CD4+	TCR+CD8+	TCR8+CD8+	TCR8+CD4+
Avidity (ELISpot, NTAmer)				
In vitro bulk sequential killing				
In vitro bulk T cell expansion				
In vitro single-cell killing				
In vitro antitumor function				
Overall performance				

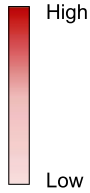

Fig. 7. TCR8$^+$CD4$^+$ T cell performance is characterized by sustained expression of diverse transcriptional programs. (**A**) Summary of the main findings identified by scRNAseq in cocultured cytotoxic engineered CD4$^+$ and CD8$^+$ T cells. (**B**) Summary of main findings from in vitro and in vivo functional assays and overall engineered T cell performance. Low to high intensity of red indicates low to high T cell function.

microenvironment but have previously not been associated with CD8 coreceptor function. To summarize our findings, we propose a working model to explain how TCR8$^+$-engineered CD4$^+$ and CD8$^+$ T cells exert their enhanced antitumor function (Fig. 7). TCR8$^+$CD4$^+$ T cells overall perform the best in our in vitro and in vivo screening assays. By scRNAseq and experimental validation, we propose that this enhanced performance is due to transcriptional changes in several pathways known to be critical for long-term antitumor activity of adoptively transferred T cells, including cytotoxicity, costimulation, metabolic programs, cell differentiation, exhaustion, and proliferation. Our study sheds light on the molecular consequences of CD8 coreceptor overexpression in combination with a transgenic tumor-targeted TCR and has the potential to guide the future development of enhanced engineered T cell therapies for clinical translation.

MATERIALS AND METHODS

Cell lines

BV173 cells were purchased from the German Cell Culture Collection (DSMZ), and K562, CEM-T2 (TAP transporter deficient), and 293T were obtained from the American Type Culture Collection (ATCC). Cells were maintained in complete RPMI 1640 or IMDM (Iscove's modified Dulbecco's medium) (Hyclone, Thermo Scientific, and Gibco) supplemented with 10 or 20% fetal bovine serum (FBS; Hyclone, Biowest, Merck, or Gibco), 1% penicillin-streptomycin (Gibco), and 1% glutaMAX (Gibco). β2-Microglobulin knockout (B2M-KO) BV173 cells were generated using the CRISPR-Cas9 technology as previously described (*54*). In brief, a B2M single-guide RNA (5′–GGCCACGGAGCGAGACAUCU–3′, Synthego) and recombinant Cas9 protein (CP01 and PNA Bio), 1 μg each, were mixed at room temperature and used to electroporate 0.15 × 10^6 BV173 cells (three pulses of 1600 V for 10 ms, Neon Transfection System, Invitrogen). Electroporated cells were expanded in antibiotic-free medium and FACS sorted to greater than 98% purity for HLA-A2–negative cells. For in vivo xenograft experiments, BV173 cells modified to express the firefly luciferase (BV173.ffLuc) cells were used as previously described (*23*).

Blood samples from healthy donors

Buffy coats were obtained from deidentified healthy human volunteers at the Gulf Coast Regional Blood Center (Houston, TX, USA) or at the Center of Interregional Blood Transfusion SRK Bern (Bern, Switzerland).

Generation of retroviral vectors and supernatant

The retroviral vector expressing the survivin-specific (s24) TCR has been previously described (*23*). Genes encoding for the human CD8α (Uniprot P01732) and CD8β isoform 1 (βM1, Uniprot P10966-1) chains, separated by a 2A sequence, were synthesized by GeneArt (Invitrogen). They were either cloned as such into the SFG retroviral vector backbone or in combination with the TCR, resulting in a polycystronic vector expressing all four genes, separated by different 2A sequences (Fig. 1A) (In-Fusion HD Cloning Kit, Clontech). Transient retroviral supernatant was prepared by transfection of 293T as described (*36*).

Generation of transgenic T cells

Peripheral blood mononuclear cells (PBMCs) were isolated from healthy donor buffy coats using density gradient centrifugation by Lymphoprep (Accurate Chemical and Scientific Corporation). Polyclonal CD4$^+$ and CD8$^+$ T cells were positively selected from PBMCs with microbeads (Miltenyi Biotech or STEMCELL Technologies Inc.) and activated in non–tissue culture–treated 24-well plates (Corning) coated with OKT3 (purified from hybridoma CRL-8001,

ATCC, or BioLegend) and anti-CD28 antibody (BD Biosciences or BioLegend), and IL-7 and IL-15 (10 ng/ml each; R&D Systems or Miltenyi) for 3 days and transduced as described (*36*). Cells were expanded for 7 to 10 days after retroviral transduction in IL-7 and IL-15 before use in experiments. T cells were cultured in a 1:1 mixture of RPMI 1640 and Click's media (Hyclone) or RPMI, complete with 10% FBS (Hyclone, Biowest, Merck, or Gibco), 1% penicillin-streptomycin, and 1% GlutaMAX.

Immunophenotyping

Extracellular surface staining was performed with antibodies or dextramer listed in table S4 for 30 min at 4°C. 7-AAD (7-amino-actinomycin D) (BD Biosciences), DAPI (4′,6-diamidino-2-phenylindole), or Zombie UV (BioLegend) was used to exclude dead cells. To evaluate LCK phosphorylation, T cells were stimulated with BV173 cells (1:1 ratio) or *Staphylococcus aureus* enterotoxin B (0.1 μg/ml; Millipore Sigma, as a positive control) for 30 min at 37°C. Indirect intracellular staining was performed using anti-human phospho-LCK (Y394) (clone: 755103, R&D Systems) and anti-mouse IgG-NL557 Abs (R&D Systems) according to the manufacturer's recommendations. Intracellular staining for all other markers was performed by first blocking cytokine secretion with GolgiStop and GolgiPlug (BD Biosciences) followed by dividing cells into three groups: (1) nonstimulated, (2) stimulated with PMA (10 ng/ml) and ionomycin (500 ng/ml), and (3) stimulated with BV173 cells at a 1:1 ratio. Cells from each condition were incubated for 4 hours at 37°C and subsequently stained for extracellular markers (table S4). After fixation and permeabilization with Cytofix/Cytoperm (BD Biosciences), cells were washed with FACS buffer containing 0.1% saponin and stained for intracellular markers (table S4). Groups 1 and 2 served as negative and positive control for the staining respectively, while data from group 3 were used for the report of intracellular proteins. To analyze the mitochondrial mass, T cells were treated with or without 10 μM oligomycin A for 2.5 hours and then stained with 100 nM MitoTracker Green (Thermo Fisher Scientific) for 15 min at 37°C for mitochondrial mass. Anti-hCD4 (clone: RPA-T4, BioLegend), anti-hCD8α (clone: SK1, BioLegend), and LIVE/DEAD Violet Stain (Thermo Fisher Scientific) were used to set analysis gates. Samples were acquired on a FACSCanto or SORP-LSRII (BD Biosciences) with BD FACSDiva software and analyzed with FlowJo software (Tree Star Inc.).

Peptides and IFN-γ ELISpot

The survivin variant peptide $LMLGEFLKL^{(96–104)}$ was obtained from Genemed Synthesis. T cells (10^5 TCR transgenic T cells) were plated in triplicates and stimulated 1:1 with peptide pulsed CEM-T2 cells (10^{-4} to 10^{-10} M). Plates were incubated at 37°C/5% CO_2 overnight and developed as previously described (*23*); spot-forming cells (SFCs) were enumerated by ZellNet.

Sequential coculture assay

T cells and BV173 cells were cocultured in four replicate wells at E:T ratio of 1:5 with no exogenous cytokines. Coculture supernatants were harvested 24 hours after initial plating and stored at −80°C for cytokine analysis. Every 3 to 4 days of coculture, remaining T cells and BV173 cells were enumerated by FACS and CountBright beads (Life Technologies). To assess the sequential killing ability of the remaining T cells, fresh BV173 cells (1×10^6) were added back to untouched replicate wells if less than 1×10^5 residual tumor cells remained per well.

Cytokine multiplex assay

Cytokine concentrations in coculture supernatants were quantified in duplicates using the MILLIPLEX Human $CD8^+$ T Cell Magnetic Bead Panel (EMD Millipore) and analyzed with the Luminex 200 instrument (Luminex).

NTAmer staining and kinetic TCR-ligand dissociation assay

Two-color reversible NTAmers were synthesized and used for off-rates measurements as described (*24*). T cells were incubated for 40 min at 4°C with HLA-A*02:01/$survivin^{LML}{}_{96–104}$–specific (LMLGEFLKL) NTAmers, composed of Cy5-labeled pMHC monomers and streptavidin–phycoerythrin (PE) scaffolds. After washing, 2×10^5 T cells were suspended in 200 μl of ice-cold FACS buffer. Baseline geometric mean fluorescence (Cy5) was first measured for 30 s under constant temperature control using a thermostat device (4°C) on a SORP-LSR II flow cytometer (BD Biosciences), following gating on fluorescein isothiocyanate–conjugated live transgenic TCR^+ T cells. Upon addition of imidazole (200 mM), the streptavidin-PE NTA_4 scaffold molecules rapidly decay (2 to 3 s), enabling direct measurements of the Cy5-pMHC monomeric dissociation from the TCR complex, which were recorded during 2 min at 4°C. Data were processed using the kinetic module of FlowJo software (v.9.6, Tree Star Inc.) as described previously (*24*). Normalized (Cy5) gMFI values for each cell type were plotted against time (s) after substraction of nonspecific background staining from the respective nontransduced CD4 and CD8 T cells (GraphPad Prism v6). Monomeric dissociation rates best fitted a one-phase exponential decay equation, from which k_{off} and half-lives ($t_{1/2}$) were determined.

Time-lapse imaging microscopy in nanowell grids

The fabrication of nanowell arrays and the single-cell cytotoxicity assay were performed as described previously (*32*, *55*). Briefly, the nanowell array was fixed on a 50-mm glass-bottom petri dish (Ted Pella). T cells (effector) and BV173 cells (target) were labeled with PKH67 Green and PKH26 Red dyes (2 μM; Sigma-Aldrich), respectively. Effectors and targets were then loaded sequentially onto nanowell arrays (10^6 cells/ml), and the array was incubated at 37°C/5% CO_2, in phenol red–free media containing annexin V Alexa Fluor 647 (Invitrogen). The cells were monitored using an Axio Observer (Carl Zeiss) fitted with a Hamamatsu digital scientific CMOS camera using a 20× 0.8 numerical aperture objective for 9 hours at 5-min intervals. The images were processed using a combination of manual tracking and the implementation of an in-house algorithm for cell tracking and segmentation (*31*).

Mouse xenograft model

Female NOD-SCID-$\gamma c^{-/-}$ (NSG) mice (6 to 8 weeks old) were purchased from the Jackson laboratory and housed at the Baylor College of Medicine Animal Facility. Sublethally irradiated (120 cGy) mice were infused intravenously (tail vein) with 3×10^6 BV173.ffluc cells per mouse 4 to 6 hours later. Leukemia burden was monitored by bioluminescence imaging (BLI) (photons/second/cm^2/sr) using the Xenogen in vivo imaging system (IVIS) (Caliper Life Sciences). Three T cell infusions (5×10^6 transgenic cells or controls per mouse, every 2 to 3 days) were administered intravenously (tail vein or retro-orbital) beginning 24 hours after tumor injection. Leukemia growth was monitored weekly by BLI.

Study approval

All animal studies were reviewed and approved by the Institutional Animal Care and Use Committee (IACUC) of Baylor College of Medicine.

Statistics

Data were summarized using descriptive statistics. Areas under the curves (AUCs) were calculated using trapezoidal rule for T cell frequencies and bioluminescence intensity over time. Comparisons were made between groups using *t* test for continuous variables. Normality assumption was examined, and log transformation was performed if necessary to achieve normality. Alternatively, Mann-Whitney *U* test (nonparametric *t* test) was applied on data with no normal distribution. Survival analysis was carried out using the Kaplan-Meier method. The log-rank test was used to analyze TIMING assay results. GraphPad Prism 5 or higher (GraphPad Software Inc., La Jolla, CA), SAS 9.4, and R 3.3.2 were used for statistical analysis. *P* values <0.05 were considered statistically significant.

Sample preparation for scRNAseq

PBMCs from one healthy donor buffy coat were isolated by density gradient centrifugation with Lymphoprep. Polyclonal $CD4^+$ and $CD8^+$ cells were positively selected with microbeads (STEMCELL Technologies) (day 0). For the analysis of "fresh" cells, $CD4^+$ and $CD8^+$ selected cells were cryopreserved on day 0 and thawed for scRNAseq on day 21. They were processed for scRNAseq at the same time as the T cells isolated from the "cocultured" condition. For the analysis of "expanded" cells, $CD4^+$ and $CD8^+$ selected cells were activated on non–tissue culture–treated plates coated with OKT3 and anti-CD28 antibody in the presence of IL-7 and IL-15 (10 ng/ml) for 3 days. Cells were then transduced with retroviral supernatants and expanded in media with IL-7/15. On day 9, transgenic cells were enriched by positive selection after staining with anti-mouse TCR PE antibody (BioLegend) and anti-PE microbeads (Miltenyi), further expanded until day 14, and processed for scRNAseq. For the analysis of cocultured cells, transgenic T cells were cocultured with BV173 cells at an effector-to-target ratio of 1:1 for 4 days (from day 17 to 21). FACS analysis was performed to assess tumor cell killing. In conditions with complete tumor cell killing ($TCR8^+CD4^+$ and $TCR8^+CD8^+$ T cells), dead cells and debris were removed with a dead cell removal kit (Miltenyi). In the case of residual tumor cells (TCR^+CD8^+ T cell condition), residual $CD19^+$ BV173 cells were removed with CD19 magnetic beads (Miltenyi). TCR^+CD4^+ T cells did not kill leukemia cells and could not be analyzed by scRNAseq due to tumor cell overgrowth. Figure 2A summarizes the experimental setup.

Sample processing, library preparation, and sequencing

Cells for scRNAseq were processed at two time points, day 14 (expanded cells, four samples) and day 21 (fresh and cocultured cells, five samples). After cell purification, T cells were resuspended in RPMI supplemented with 10% FBS, strained to remove aggregates, and loaded into a Chromium Single Cell Controller (10× Genomics, Pleasanton, CA) in a chip together with beads, master mix reagents (containing RT enzyme and poly-dt RT primers), and oil to generate single-cell–containing droplets. Single-cell gene expression libraries were then prepared using Chromium Single Cell 3′ Library & Gel Bead Kit v2 (PN-120267) following the manufacturer's instruction (protocol CG00052 Rev. E). Quality control was performed with a TapeStation 4200 (Agilent) and QuBit double-stranded DNA high-sensitivity assay (Thermo Fisher Scientific) following the manufacturer's instructions. Encapsulation and library preparation were performed at the genomics facility of the Ecole Polytechnique Federale de Lausanne. Next-generation sequencing was performed at the iGE3 Genomics Platform at the University of Geneva on a HiSeq 4000 (Illumina), using a PE100-100 sequencing configuration.

scRNAseq data analysis

Data processing on cellRanger software

Mapping, counting, and aggregation of sequencing reads were performed in cellRanger software v2.2.0 (10X Genomics). The human genome "GRCh38" was modified to include the sequences for the TCR and CD8αβ transgenes using the function "mkref" with modified fasta and gtf files. The function "count" was used for read alignment and count estimation, the parameter "--expect-cells" was used with the respective number of processed cells for each sample, and cells were selected with the default UMI (unique molecular identifier) filter method. The samples were aggregated using the function "aggr" with default parameters. The data were converted into a SingleCellExperiment object from the SingleCellExperiment R package.

Quality control and data normalization

Cells with more than 5 mitochondrial genes or less than 10 ribosomal genes were filtered out, as well as 273 cells from two small populations that were annotated as B cells or dendritic cells, leading to a total of 25,474 T cells for analysis. Genes expressed in less than 10 cells were removed leaving 16,858 genes in the dataset for analysis. Gene expression was normalized with the R package "scran." The parameters "min.mean=0.1" and "min.size=100" were used for the "quickCluster." Sum factors were computed with "min.mean=0.1" and used for normalization. Because of important differences in total number of reads between samples, we further used housekeeping (HK) genes for normalization. Median expressions of five HK genes ("*C1orf43*," "*PSMB4*," "*RAB7A*," "*SNRPD3*," and "*VPS29*") in each sample were calculated, and the average was used as normalizing factors specific for each sample (*56*).

Dimension reductions

Dimension reductions were performed using the R package "scater" (*57*). Principal components analysis (PCA) was performed using the function "runPCA" with the following parameters: "ncomponents=50," "ntop=1000," "method=irlba," and "scale_features=FALSE." Next, t-SNE was performed using the function "runTSNE" with the following parameters: "perplexity=90," "use_dimred = 'PCA'," "normalize=FALSE," and "scale_features=FALSE." On the basis of the t-SNE coordinates, the cells were clustered using the function "buildSNNGraph" from the R package "scran," with the parameter "k=100."

Differential gene expression

All differential expression analyses were performed in "Seurat" (*58*). The function "FindMarkers" was used for pairwise comparison between groups of cells (samples or clusters). A log fold change (fc) threshold of 0.25 (~1.28 fc) was applied in later steps to select genes as DE.

Analysis of T cell differentiation subsets

To identify the T cell differentiation subsets (T_N, T_{CM}, T_{EM}, and T_{EFF}), we only considered genes with known progressive expression change across subsets (*30*). From the 457 genes listed in the paper by Gattinoni *et al.* (*30*), we selected the genes expressed in at least 10% of all single cells of our samples (table S3). In addition, the genes annotated to the gene ontology term "cell cycle" (GO_0007049) were filtered out. This led to a final list of 178 genes, which were used for subsequent clustering. Pearson correlation was calculated between all cells within groups defined by their cell type and state: CD4 or CD8 fresh, CD4 or CD8 expanded, and CD4 or CD8 cocultured.

For each group, the cells were clustered using hierarchical clustering with "ward.D2" method and selecting k=4 clusters. To associate each cluster to a subcellular type, the mean expression of a list of genes known to vary between T_N, T_{CM}, T_{EM}, and T_{EFF} (table S3) was used, and these genes were ranked from #1 to #4 across the four clusters in each sample. In each sample, the clusters were assigned to cell states based on the optimal correspondence with the ranking of the genes in our list (fig. S6).

Data visualization

Figures were generated in R with the "ggplot2" package. t-SNE plots for gene markers were complemented with contour lines (function "geom_density_2d") to highlight the regions with the highest gene expression. Violin plots were generated in "scater" using the function "plotExpression." Results of enrichment analyses were plotted using the function "dotplot" (*59*). Gene sets were built for a large set of signatures, ranging from cell state and type, to molecular function and biological process (pathways). The sets for metabolic pathways were obtained from the Kyoto Encyclopedia of Genes and Genomes (KEGG) (https://www.genome.jp/kegg/) or reactome (https://reactome.org) databases. Gene sets used for characterization of T cell phenotypes are summarized in table S3.

SUPPLEMENTARY MATERIALS

Supplementary material for this article is available at http://advances.sciencemag.org/cgi/content/full/6/27/eaaz7809/DC1

REFERENCES AND NOTES

1. E. C. Morris, A. Tsallios, G. M. Bendle, S.-A. Xue, H. J. Stauss, A critical role of T cell antigen receptor-transduced MHC class I-restricted helper T cells in tumor protection. *Proc. Natl. Acad. Sci. U.S.A.* **102**, 7934–7939 (2005).
2. H. W. Kessels, K. Schepers, M. D. van den Boom, D. J. Topham, T. N. Schumacher, Generation of T cell help through a MHC class I-restricted TCR. *J. Immunol.* **177**, 976–982 (2006).
3. T. L. Frankel, W. R. Burns, P. D. Peng, Z. Yu, D. Chinnasamy, J. A. Wargo, Z. Zheng, N. P. Restifo, S. A. Rosenberg, R. A. Morgan, Both CD4 and CD8 T cells mediate equally effective in vivo tumor treatment when engineered with a highly avid TCR targeting tyrosinase. *J. Immunol.* **184**, 5988–5998 (2010).
4. S.-A. Xue, L. Gao, M. Ahmadi, S. Ghorashian, R. D. Barros, C. Pospori, A. Holler, G. Wright, S. Thomas, M. Topp, E. C. Morris, H. J. Stauss, Human MHC Class I-restricted high avidity $CD4^+$ T cells generated by co-transfer of TCR and CD8 mediate efficient tumor rejection in vivo. *Oncoimmunology* **2**, e22590 (2013).
5. M. M. van Loenen, R. S. Hagedoorn, R. de Boer, J. H. Falkenburg, M. H. Heemskerk, Extracellular domains of CD8α and CD8ß subunits are sufficient for HLA class I restricted helper functions of TCR-engineered $CD4^+$ T cells. *PLOS ONE* **8**, e65212 (2013).
6. R. G. Dossa, T. Cunningham, D. Sommermeyer, I. Medina-Rodriguez, M. A. Biernacki, K. Foster, M. Bleakley, Development of T-cell immunotherapy for hematopoietic stem cell transplantation recipients at risk of leukemia relapse. *Blood* **131**, 108–120 (2018).
7. B. Laugel, D. K. Cole, M. Clement, L. Wooldridge, D. A. Price, A. K. Sewell, The multiple roles of the CD8 coreceptor in T cell biology: Opportunities for the selective modulation of self-reactive cytotoxic T cells. *J. Leukoc. Biol.* **90**, 1089–1099 (2011).
8. D. K. Cole, B. Laugel, M. Clement, D. A. Price, L. Wooldridge, A. K. Sewell, The molecular determinants of CD8 co-receptor function. *Immunology* **137**, 139–148 (2012).
9. L. Wooldridge, H. A. van den Berg, M. Glick, E. Gostick, B. Laugel, S. L. Hutchinson, A. Milicic, J. M. Brenchley, D. C. Douek, D. A. Price, A. K. Sewell, Interaction between the CD8 coreceptor and major histocompatibility complex class I stabilizes T cell receptor-antigen complexes at the cell surface. *J. Biol. Chem.* **280**, 27491–27501 (2005).
10. I. F. Luescher, E. Vivier, A. Layer, J. Mahiou, F. Godeau, B. Malissen, P. Romero, CD8 modulation of T-cell antigen receptor-ligand interactions on living cytotoxic T lymphocytes. *Nature* **373**, 353–356 (1995).
11. A. M. Norment, R. D. Salter, P. Parham, V. H. Engelhard, D. R. Littman, Cell-cell adhesion mediated by CD8 and MHC class I molecules. *Nature* **336**, 79–81 (1988).
12. A. Veillette, M. A. Bookman, E. M. Horak, J. B. Bolen, The CD4 and CD8 T cell surface antigens are associated with the internal membrane tyrosine-protein kinase $p56^{lck}$. *Cell* **55**, 301–308 (1988).
13. A. Arcaro, C. Grégoire, T. R. Bakker, L. Baldi, M. Jordan, L. Goffin, N. Boucheron, F. Wurm, P. A. van der Merwe, B. Malissen, I. F. Luescher, CD8β endows CD8 with efficient coreceptor function by coupling T cell receptor/CD3 to raft-associated $CD8/p56^{lck}$ complexes. *J. Exp. Med.* **194**, 1485–1495 (2001).
14. D. J. Pang, A. C. Hayday, M.-J. Bijlmakers, CD8 Raft localization is induced by its assembly into CD8αβ heterodimers, not CD8αα homodimers. *J. Biol. Chem.* **282**, 13884–13894 (2007).
15. A. Arcaro, C. Grégoire, N. Boucheron, S. Stotz, E. Palmer, B. Malissen, I. F. Luescher, Essential role of CD8 palmitoylation in CD8 coreceptor function. *J. Immunol.* **165**, 2068–2076 (2000).
16. P. D. Holler, D. M. Kranz, Quantitative analysis of the contribution of TCR/pepMHC affinity and CD8 to T cell activation. *Immunity* **18**, 255–264 (2003).
17. A.-M. McNicol, G. Bendle, A. Holler, T. Matjeka, E. Dalton, L. Rettig, R. Zamoyska, W. Uckert, S.-A. Xue, H. J. Stauss, CD8α/α homodimers fail to function as co-receptor for a CD8-dependent TCR. *Eur. J. Immunol.* **37**, 1634–1641 (2007).
18. L. Wooldridge, B. Laugel, J. Ekeruche, M. Clement, H. A. van den Berg, D. A. Price, A. K. Sewell, CD8 controls T cell cross-reactivity. *J. Immunol.* **185**, 4625–4632 (2010).
19. R. Kennedy, E. Celis, Multiple roles for $CD4^+$ T cells in anti-tumor immune responses. *Immunol. Rev.* **222**, 129–144 (2008).
20. E. A. Walter, P. D. Greenberg, M. J. Gilbert, R. J. Finch, K. S. Watanabe, E. D. Thomas, S. R. Riddell, Reconstitution of cellular immunity against cytomegalovirus in recipients of allogeneic bone marrow by transfer of T-cell clones from the donor. *N. Engl. J. Med.* **333**, 1038–1044 (1995).
21. E. Tran, P. F. Robbins, Y.-C. Lu, T. D. Prickett, J. J. Gartner, L. Jia, A. Pasetto, Z. Zheng, S. Ray, E. M. Groh, I. R. Kriley, S. A. Rosenberg, T-cell transfer therapy targeting mutant KRAS in cancer. *N. Engl. J. Med.* **375**, 2255–2262 (2016).
22. C. J. Turtle, L.-A. Hanafi, C. Berger, M. Hudecek, B. Pender, E. Robinson, R. Hawkins, C. Chaney, S. Cherian, X. Chen, L. Soma, B. Wood, D. Li, S. Heimfeld, S. R. Riddell, D. G. Maloney, Immunotherapy of non-Hodgkin's lymphoma with a defined ratio of $CD8^+$ and $CD4^+$ CD19-specific chimeric antigen receptor-modified T cells. *Sci. Transl. Med.* **8**, 355ra116 (2016).
23. C. Arber, X. Feng, H. Abhyankar, E. Romero, M.-F. Wu, H. E. Heslop, P. Barth, G. Dotti, B. Savoldo, Survivin-specific T cell receptor targets tumor but not T cells. *J. Clin. Invest.* **125**, 157–168 (2015).
24. M. Hebeisen, J. Schmidt, P. Guillaume, P. Baumgaertner, D. E. Speiser, I. Luescher, N. Rufer, Identification of rare high-avidity, tumor-reactive $CD8^+$ T cells by monomeric TCR-ligand off-rates measurements on living cells. *Cancer Res.* **75**, 1983–1991 (2015).
25. M. Hebeisen, M. Allard, P. O. Gannon, J. Schmidt, D. E. Speiser, N. Rufer, Identifying individual T cell receptors of optimal avidity for tumor antigens. *Front. Immunol.* **6**, 582 (2015).
26. F. Yu, S. Sharma, D. Jankovic, R. K. Gurram, P. Su, G. Hu, R. Li, S. Rieder, K. Zhao, B. Sun, J. Zhu, The transcription factor Bhlhe40 is a switch of inflammatory versus antiinflammatory Th1 cell fate determination. *J. Exp. Med.* **215**, 1813–1821 (2018).
27. C.-C. Lin, T. R. Bradstreet, E. A. Schwarzkopf, J. Sim, J. A. Carrero, C. Chou, L. E. Cook, T. Egawa, R. Taneja, T. L. Murphy, J. H. Russell, B. T. Edelson, Bhlhe40 controls cytokine production by T cells and is essential for pathogenicity in autoimmune neuroinflammation. *Nat. Commun.* **5**, 3551 (2014).
28. L. Nötzold, L. Frank, M. Gandhi, M. Polycarpou-Schwarz, M. Groß, M. Gunkel, N. Beil, H. Erfle, N. Harder, K. Rohr, J. Trendel, J. Krijgsveld, T. Longerich, P. Schirmacher, M. Boutros, S. Erhardt, S. Diederichs, The long non-coding RNA LINC00152 is essential for cell cycle progression through mitosis in HeLa cells. *Sci. Rep.* **7**, 2265 (2017).
29. Y. Serroukh, C. Gu-Trantien, B. Hooshiar Kashani, M. Defrance, T.-P. Vu Manh, A. Azouz, A. Detavernier, A. Hoyois, J. Das, M. Bizet, E. Pollet, T. Tabbuso, E. Calonne, K. van Gisbergen, M. Dalod, F. Fuks, S. Goriely, A. Marchant, The transcription factors Runx3 and ThPOK cross-regulate acquisition of cytotoxic function by human Th1 lymphocytes. *eLife* **7**, e30496 (2018).
30. L. Gattinoni, E. Lugli, Y. Ji, Z. Pos, C. M. Paulos, M. F. Quigley, J. R. Almeida, E. Gostick, Z. Yu, C. Carpenito, E. Wang, D. C. Douek, D. A. Price, C. H. June, F. M. Marincola, M. Roederer, N. P. Restifo, A human memory T cell subset with stem cell–like properties. *Nat. Med.* **17**, 1290–1297 (2011).
31. A. Merouane, N. Rey-Villamizar, Y. Lu, I. Liadi, G. Romain, J. Lu, H. Singh, L. J. N. Cooper, N. Varadarajan, B. Roysam, Automated profiling of individual cell–cell interactions from high-throughput time-lapse imaging microscopy in nanowell grids (TIMING). *Bioinformatics* **31**, 3189–3197 (2015).
32. I. Liadi, H. Singh, G. Romain, N. Rey-Villamizar, A. Merouane, J. R. T. Adolacion, P. Kebriaei, H. Huls, P. Qiu, B. Roysam, L. J. N. Cooper, N. Varadarajan, Individual motile $CD4^+$ T cells can participate in efficient multikilling through conjugation to multiple tumor cells. *Cancer Immunol. Res.* **3**, 473–482 (2015).
33. L. Chen, D. B. Flies, Molecular mechanisms of T cell co-stimulation and co-inhibition. *Nat. Rev. Immunol.* **13**, 227–242 (2013).
34. O. U. Kawalekar, R. S. O'Connor, J. A. Fraietta, L. Guo, S. E. McGettigan, A. D. Posey Jr., P. R. Patel, S. Guedan, J. Scholler, B. Keith, N. W. Snyder, I. A. Blair, M. C. Milone, C. H. June,

Distinct signaling of coreceptors regulates specific metabolism pathways and impacts memory development in CAR T cells. *Immunity* **44**, 380–390 (2016).
35. N. Jones, J. G. Cronin, G. Dolton, S. Panetti, A. J. Schauenburg, S. A. E. Galloway, A. K. Sewell, D. K. Cole, C. A. Thornton, N. J. Francis, Metabolic adaptation of human $CD4^+$ and $CD8^+$ T-cells to T-cell receptor-mediated stimulation. *Front. Immunol.* **8**, 1516 (2017).
36. C. D. Nishimura, D. A. Brenner, M. Mukherjee, R. A. Hirsch, L. Ott, M.-F. Wu, H. Liu, O. Dakhova, J. S. Orange, M. K. Brenner, C. Y. Lin, C. Arber, c-MPL provides tumor-targeted T-cell receptor-transgenic T cells with costimulation and cytokine signals. *Blood* **130**, 2739–2749 (2017).
37. O. S. Kustikova, A. Wahlers, K. Kühlcke, B. Stähle, A. R. Zander, C. Baum, B. Fehse, Dose finding with retroviral vectors: Correlation of retroviral vector copy numbers in single cells with gene transfer efficiency in a cell population. *Blood* **102**, 3934–3937 (2003).
38. M. Ahmadi, J. W. King, S.-A. Xue, C. Voisine, A. Holler, G. P. Wright, J. Waxman, E. Morris, H. J. Stauss, CD3 limits the efficacy of TCR gene therapy in vivo. *Blood* **118**, 3528–3537 (2011).
39. R. I. Klein Geltink, D. O'Sullivan, M. Corrado, A. Bremser, M. D. Buck, J. M. Buescher, E. Firat, X. Zhu, G. Niedermann, G. Caputa, B. Kelly, U. Warthorst, A. Rensing-Ehl, R. L. Kyle, L. Vandersarren, J. D. Curtis, A. E. Patterson, S. Lawless, K. Grzes, J. Qiu, D. E. Sanin, O. Kretz, T. B. Huber, S. Janssens, B. N. Lambrecht, A. S. Rambold, E. J. Pearce, E. L. Pearce, Mitochondrial priming by CD28. *Cell* **171**, 385–397.e11 (2017).
40. K. A. Frauwirth, J. L. Riley, M. H. Harris, R. V. Parry, J. C. Rathmell, D. R. Plas, R. L. Elstrom, C. H. June, C. B. Thompson, The CD28 signaling pathway regulates glucose metabolism. *Immunity* **16**, 769–777 (2002).
41. L. A. Callender, E. C. Carroll, E. A. Bober, A. N. Akbar, E. Solito, S. M. Henson, Mitochondrial mass governs the extent of human T cell senescence. *Aging Cell* **19**, e13067 (2020).
42. L. Zhang, P. Romero, Metabolic control of $CD8^+$ T cell fate decisions and antitumor immunity. *Trends Mol. Med.* **24**, 30–48 (2018).
43. D. L. Wiest, L. Yuan, J. Jefferson, P. Benveniste, M. Tsokos, R. D. Klausner, L. H. Glimcher, L. E. Samelson, A. Singer, Regulation of T cell receptor expression in immature CD4+CD8+ thymocytes by p56lck tyrosine kinase: Basis for differential signaling by CD4 and CD8 in immature thymocytes expressing both coreceptor molecules. *J. Exp. Med.* **178**, 1701–1712 (1993).
44. I. Xhangolli, B. Dura, G. Lee, D. Kim, Y. Xiao, R. Fan, Single-cell analysis of CAR-T cell activation reveals a mixed T_H1/T_H2 response independent of differentiation. *Genomics Proteomics Bioinformatics* **17**, 129–139 (2019).
45. C. Berger, M. C. Jensen, P. M. Lansdorp, M. Gough, C. Elliott, S. R. Riddell, Adoptive transfer of effector $CD8^+$ T cells derived from central memory cells establishes persistent T cell memory in primates. *J. Clin. Invest.* **118**, 294–305 (2008).
46. N. Cieri, B. Camisa, F. Cocchiarella, M. Forcato, G. Oliveira, E. Provasi, A. Bondanza, C. Bordignon, J. Peccatori, F. Ciceri, M. T. Lupo-Stanghellini, F. Mavilio, A. Mondino, S. Bicciato, A. Recchia, C. Bonini, IL-7 and IL-15 instruct the generation of human memory stem T cells from naive precursors. *Blood* **121**, 573–584 (2013).
47. P. Graef, V. R. Buchholz, C. Stemberger, M. Flossdorf, L. Henkel, M. Schiemann, I. Drexler, T. Höfer, S. R. Riddell, D. H. Busch, Serial transfer of single-cell-derived immunocompetence reveals stemness of $CD8^+$ central memory T cells. *Immunity* **41**, 116–126 (2014).
48. L. Gattinoni, D. E. Speiser, M. Lichterfeld, C. Bonini, T memory stem cells in health and disease. *Nat. Med.* **23**, 18–27 (2017).
49. I. B. Mazo, M. Honczarenko, H. Leung, L. L. Cavanagh, R. Bonasio, W. Weninger, K. Engelke, L. Xia, R. P. McEver, P. A. Koni, L. E. Silberstein, U. H. von Andrian, Bone marrow is a major reservoir and site of recruitment for central memory $CD8^+$ T cells. *Immunity* **22**, 259–270 (2005).
50. D. Ostroumov, N. Fekete-Drimusz, M. Saborowski, F. Kühnel, N. Woller, CD4 and CD8 T lymphocyte interplay in controlling tumor growth. *Cell. Mol. Life Sci.* **75**, 689–713 (2018).
51. E. Tran, S. Turcotte, A. Gros, P. F. Robbins, Y.-C. Lu, M. E. Dudley, J. R. Wunderlich, R. P. Somerville, K. Hogan, C. S. Hinrichs, M. R. Parkhurst, J. C. Yang, S. A. Rosenberg, Cancer immunotherapy based on mutation-specific CD4+ T cells in a patient with epithelial cancer. *Science* **344**, 641–645 (2014).
52. R. A. Gardner, O. Finney, C. Annesley, H. Brakke, C. Summers, K. Leger, M. Bleakley, C. Brown, S. Mgebroff, K. S. Kelly-Spratt, V. Hoglund, C. Lindgren, A. P. Oron, D. Li, S. R. Riddell, J. R. Park, M. C. Jensen, Intent-to-treat leukemia remission by CD19 CAR T cells of defined formulation and dose in children and young adults. *Blood* **129**, 3322–3331 (2017).
53. D. Wang, B. Aguilar, R. Starr, D. Alizadeh, A. Brito, A. Sarkissian, J. R. Ostberg, S. J. Forman, C. E. Brown, Glioblastoma-targeted $CD4^+$ CAR T cells mediate superior antitumor activity. *JCI Insight* **3**, e99048 (2018).
54. M. C. Gundry, L. Brunetti, A. Lin, A. E. Mayle, A. Kitano, D. Wagner, J. I. Hsu, K. A. Hoegenauer, C. M. Rooney, M. A. Goodell, D. Nakada, Highly efficient genome editing of murine and human hematopoietic progenitor cells by CRISPR/Cas9. *Cell Rep.* **17**, 1453–1461 (2016).
55. G. Romain, V. Senyukov, N. Rey-Villamizar, A. Merouane, W. Kelton, I. Liadi, A. Mahendra, W. Charab, G. Georgiou, B. Roysam, D. A. Lee, N. Varadarajan, Antibody Fc engineering improves frequency and promotes kinetic boosting of serial killing mediated by NK cells. *Blood* **124**, 3241–3249 (2014).
56. E. Eisenberg, E. Y. Levanon, Human housekeeping genes, revisited. *Trends Genet.* **29**, 569–574 (2013).
57. D. J. McCarthy, K. R. Campbell, A. T. Lun, Q. F. Wills, Scater: Pre-processing, quality control, normalization and visualization of single-cell RNA-seq data in R. *Bioinformatics* **33**, 1179–1186 (2017).
58. R. Satija, J. A. Farrell, D. Gennert, A. F. Schier, A. Regev, Spatial reconstruction of single-cell gene expression data. *Nat. Biotechnol.* **33**, 495–502 (2015).
59. H. Wickham, *ggplot2: Elegant Graphics for Data Analysis* (Springer Science & Business Media, 2009).

Acknowledgments: We thank P. Romero for the critical reading of the manuscript. **Funding:** J.A.R. is a recipient of a Swiss Government Excellence Scholarship. N.V. is supported by NIH (R01CA174385), CPRIT (RP180466), MRA award (509800), Owens Foundation, CDMRP (CA160591), and NSF (1705464). P.-C.H. is supported by the Swiss National Science Foundation (SNSF) (31003A_182470), the Swiss Institute for Experimental Cancer Research (ISREC 26075483), a European Research Council Starting Grant (802773-MitoGuide), and the Cancer Research Institute Clinic and Laboratory Integration Program. D.G. is supported by the SNSF (31003A_173156). C.A. is supported by the Leukemia & Lymphoma Society (LLS) Translational Research Program grant (6490-16), a CPRIT Individual Investigator Research Award (RP160345), a Swiss Cancer Research grant KFS-4542-08-2018-R, and the Department of Oncology, Lausanne University Hospital, Ludwig Institute for Cancer Research and University of Lausanne. We also appreciate the support of shared resources from the Dan L. Duncan Comprehensive Cancer Center support grant P30CA125123. **Author contributions:** J.A.R. and G.B. designed research, performed experiments, analyzed and interpreted the results, and wrote the manuscript. B.C. performed scRNAseq data analysis and edited the manuscript. E.H., I.G., Y.-R.Y., and N.N. performed experiments and analyzed the results. M.W. and T.W. performed the statistical analysis. M.A.M.-P., F.S., and N.V. performed TIMING assay and analyzed and interpreted the results. M.H. and N.R. performed and interpreted the NTAmer assay and edited the manuscript. P.-C.H. interpreted the results. M.K.B. discussed the study design and results and edited the manuscript. D.G. designed and supervised the scRNAseq data analysis and edited the manuscript. C.A. designed the research and supervised the entire study, performed experiments, analyzed and interpreted the results, and wrote the manuscript. All authors reviewed and approved the final version of the manuscript. **Competing interests:** G.B., M.K.B., and C.A. have pending patent applications in the field of engineered T cell therapies. M.K.B. has equity interest and SAB membership of TScan, Marker Therapeutics, and Allovir. N.V. has pending patents on the TIMING methodology and is founder and CSO of CellChorus. P.-C.H. is on the SAB of Elixirion Immunotherapeutics and receives research support from Roche-pRED and honoraria from Pfizer and Chugai. The authors declare that they have no other competing interests. **Data and materials availability:** We deposited the scRNAseq data in the NCBI Gene Expression Omnibus (GEO) database with accession number GSE132164. All data needed to evaluate the conclusions in the paper are present in the paper and/or the Supplementary Materials. Additional data related to this paper may be requested from the authors.

Submitted 8 October 2019
Accepted 26 May 2020
Published 3 July 2020
10.1126/sciadv.aaz7809

Citation: J. A. Rath, G. Bajwa, B. Carreres, E. Hoyer, I. Gruber, M. A. Martínez-Paniagua, Y.-R. Yu, N. Nouraee, F. Sadeghi, M. Wu, T. Wang, M. Hebeisen, N. Rufer, N. Varadarajan, P.-C. Ho, M. K. Brenner, D. Gfeller, C. Arber, Single-cell transcriptomics identifies multiple pathways underlying antitumor function of TCR- and CD8αβ-engineered human $CD4^+$ T cells. *Sci. Adv.* **6**, eaaz7809 (2020).

ScienceAdvances

Single-cell transcriptomics identifies multiple pathways underlying antitumor function of TCR- and CD8 αβ-engineered human CD4+ T cells

Jan A. Rath, Gagan Bajwa, Benoit Carreres, Elisabeth Hoyer, Isabelle Gruber, Melisa A. Martínez-Paniagua, Yi-Ru Yu, Nazila Nouraee, Fatemeh Sadeghi, Mengfen Wu, Tao Wang, Michael Hebeisen, Nathalie Rufer, Navin Varadarajan, Ping-Chih Ho, Malcolm K. Brenner, David Gfeller and Caroline Arber

Sci Adv **6** (27), eaaz7809.
DOI: 10.1126/sciadv.aaz7809